Geoscience Frontiers 10 (2019) 175–194

HOSTED BY

Contents lists available at ScienceDirect

China University of Geosciences (Beijing)

Geoscience Frontiers

journal homepage: www.elsevier.com/locate/gsf

Research Paper

Magmatism and metamorphism at ca. 1.45 Ga in the northern Gawler Craton: The Australian record of rifting within Nuna (Columbia)

Laura J. Morrissey [a,b,*], Karin M. Barovich [b], Martin Hand [b], Katherine E. Howard [b], Justin L. Payne [a]

[a] School of Natural and Built Environments, University of South Australia, Adelaide, Australia
[b] Department of Earth Sciences, School of Physical Sciences, University of Adelaide, Adelaide, SA, 5005, Australia

ARTICLE INFO

Article history:
Received 28 February 2018
Received in revised form
14 June 2018
Accepted 16 July 2018
Available online 24 August 2018
Handling Editor: M. Santosh

Keywords:
Gawler Craton
Laurentia
Metamorphism
U–Pb geochronology
Paleogeographic reconstruction

ABSTRACT

U–Pb monazite and zircon geochronology and calculated metamorphic phase diagrams from drill holes in the northern Gawler Craton, southern Australia, reveal the presence of ca. 1.45 Ga magmatism and metamorphism. Magmatism and granulite facies metamorphism of this age has not previously been recognised in the Gawler Craton. The magmatic rocks have steep LREE-enriched patterns and high Ga/Al values, suggesting they are A-type granites. Calculated metamorphic forward models suggest that this event was associated with high apparent thermal gradients and reached pressures of 3.2–5.4 kbar and temperatures of 775–815 °C. The high apparent thermal gradients may reflect pluton-enhanced metamorphism, consistent with the presence of A-type granites. The recognition of ca. 1.45 Ga tectonism in the northern Gawler Craton is added to a compilation of ca. 1.50–1.40 Ga magmatism, shear zone reactivation, rift basin development and isotope resetting throughout the South and North Australian Cratons that shows that this event was widespread in eastern Proterozoic Australia. This event is stylistically similar to ca. 1.45 Ga A-type magmatism and high thermal gradient metamorphism in Laurentia in this interval and provides further support for a connection between Australia and Laurentia during the Mesoproterozoic. The tectonic setting of the 1.50–1.40 Ga event is unclear but may record rifting within the Nuna (or Columbia) supercontinent, or a period of intracontinental extension within a long-lived convergent setting.

1. Introduction

The Nuna (or Columbia) supercontinent is proposed to have existed from ca. 1.90 Ga to ca. 1.30 Ga (e.g. Evans and Mitchell, 2011). The existence of Nuna is based on evidence including global peaks in isotopic ages (e.g. Condie and Aster, 2010), paleomagnetic constraints (e.g. Evans and Mitchell, 2011; Zhang et al., 2012; Pisarevsky et al., 2014) and the widespread occurrence of 2.10–1.80 Ga collisional orogenic belts that are suggested to record the amalgamation of Nuna (e.g. Zhao et al., 2002; Zhao et al., 2004). The supercontinent cycle and past configuration of continental blocks continues to generate interest as there are now well established links between the supercontinent cycle and secular changes in the Earth's surficial environment and climate, biogeochemical cycles, and the distribution of ore deposits through time (e.g. Groves et al., 2005; Reddy and Evans, 2009; Nance et al., 2014; Cawood and Hawkesworth, 2015; Pehrsson et al., 2015).

Current reconstructions commonly place Laurentia in the core of Nuna, configurations that are generally similar to proposed Rodinia models (e.g. Karlstrom et al., 2001; Goodge et al., 2008; Li et al., 2008b; Evans and Mitchell, 2011; Meert, 2014; Pehrsson et al., 2015). Nuna reconstructions place the North Australian Craton and Mawson Continent (including the South Australian Craton and East Antarctica; Payne et al., 2009) adjacent to western Laurentia, although the positioning of Australia along the western margin of Laurentia varies significantly between models (e.g. Zhao et al., 2002; Payne et al., 2009; Evans and Mitchell, 2011; Zhang et al., 2012; Medig et al., 2014; Pisarevsky et al., 2014; Mulder et al., 2015; Betts et al., 2016; Pehrsson et al., 2015). The timing of amalgamation of Australia and Laurentia within the Nuna

* Corresponding author. School of Natural and Built Environments, University of South Australia, Adelaide, Australia.
E-mail address: laura.morrissey@unisa.edu.au (L.J. Morrissey).
Peer-review under responsibility of China University of Geosciences (Beijing).

https://doi.org/10.1016/j.gsf.2018.07.006

supercontinent is poorly constrained, with some workers suggesting amalgamation prior to 1.74 Ga (e.g. Payne et al., 2009; Zhang et al., 2012) or as late as ca. 1.55 Ga (Pisarevsky et al., 2014), whereas others propose a complex history involving initial amalgamation at ca. 1.85–1.74 Ga, followed by ocean development and re-amalgamation after ca. 1.56 Ga (Betts and Giles, 2006; Betts et al., 2008). Similarly, the timing of the separation between Australia and Laurentia is also poorly constrained, as there are no reliable paleomagnetic constraints for Australia in the interval 1.50–1.22 Ga (Pisarevsky et al., 2014).

A further uncertainty for Nuna reconstructions is that the tectonic configuration of the Australian cratonic blocks during the Proterozoic is still debated. Most paleogeographic reconstructions place the three cratonic elements of Australia (the North, South and West Australian cratons: NAC, SAC and WAC) in proximity from the Paleoproterozoic (Li, 2000; Wingate and Evans, 2003; Betts and Giles, 2006; Cawood and Korsch, 2008). However, these cratons are now separated by ca. 1.30–1.10 Ga orogenic belts, leading some workers to suggest that Australia may not have amalgamated until the Mesoproterozoic (Myers et al., 1996; Smits et al., 2014). Many reconstructions require the SAC and associated Mawson Continent to rotate from a position adjacent to the NAC to its present position between ca. 1.50 Ga and 1.30 Ga (e.g. Giles et al., 2004; Betts and Giles, 2006; Cawood and Korsch, 2008; Payne et al., 2009). The northern Gawler Craton is therefore a key region to explore the relationship between the NAC and SAC in this interval.

This study uses LA-ICP-MS geochronology and calculated metamorphic forward models from drill hole samples in the northern Gawler Craton. Almost all the northern Gawler Craton is buried beneath thick younger cover sequences and drill hole samples provide the only information on the crystalline basement in an >150,000 km^2 area. These drill holes (sampled at depths of 180–480 m) provide evidence for previously unrecognised ca. 1.50–1.45 Ga magmatism and metamorphism in the northern Gawler Craton. Calculated metamorphic phase diagrams are used to constrain the conditions of metamorphism, which suggest that this event was associated with high thermal gradients. The ca. 1.45 Ga geochronology from the northern Gawler Craton is added to a new compilation of ca. 1.50–1.40 Ga magmatism, shear zone reactivation, cooling and isotope resetting throughout the SAC and NAC. In Laurentia, the interval 1.50–1.40 Ga involved stylistically similar, pluton-enhanced high thermal gradient metamorphism, rift basin development and voluminous A-type magmatism (e.g. Anderson and Bender, 1989; Nyman et al., 1994; Evans et al., 2000; Bickford et al., 2015). The recognition of a widespread, thermally dominated event at ca. 1.45 Ga within Australia strengthens correlations between Australia and Laurentia and has implications for Nuna reconstructions.

2. Geological setting

2.1. Precambrian Australia

Proterozoic Australia has been divided into three cratonic elements: the South, North and West Australian cratons, which are separated by regions of Mesoproterozoic tectonism (Fig. 1; Myers et al., 1996). The SAC and NAC are now separated by the Musgrave Province, which records extensive deformation and metamorphism during the ca. 1.34–1.29 Ga Mount West Orogeny and the ca. 1.22–1.12 Ga Musgrave Orogeny (Smithies et al., 2011; Kirkland et al., 2013b; Tucker et al., 2015; Walsh et al., 2015). The western margin of the SAC is now covered by extensive sedimentary cover. It is separated from the WAC by the ca. 1.30–1.10 Ga Albany–Fraser Orogen and the unexposed and poorly understood Madura and Coompana Provinces (e.g. Wade et al., 2007; Kirkland et al., 2011; Kirkland et al., 2015; Spaggiari et al., 2015; Kirkland et al., 2017). The NAC and WAC are separated by the Rudall Complex, which records a polymetamorphic history between ca. 1.80 Ga and 0.55 Ga (Smithies and Bagas, 1997; Bagas, 2004; Kirkland et al., 2013a; Tucker et al., 2018).

2.2. Gawler Craton

The Gawler Craton records a protracted geological history from ca. 3.15 Ga to ca. 1.45 Ga (Fig. 1a; Daly et al., 1998; Hand et al., 2007; Payne et al., 2009; Fraser et al., 2010; Reid and Hand, 2012). The oldest rocks in the Gawler Craton are ca. 3.25–3.15 Ga granitic gneisses that outcrop within a discrete shear-zone bounded tectonostratigraphic domain in the southeastern Gawler Craton (Fraser et al., 2010). Seismic data suggest that these rocks may form the basement to a large part of the Gawler Craton (Fraser et al., 2010; Reid and Hand, 2012). The Neoarchean to earliest Paleoproterozoic Mulgathing Complex in the central-western Gawler Craton and the Sleaford Complex in the southern Gawler Craton are interpreted to represent portions of a single Late Archean belt. They dominantly comprise ca. 2.56–2.48 Ga volcanic and sedimentary successions and 2.52–2.42 Ga intrusives (Swain et al., 2005a; Reid and Hand, 2012; Reid et al., 2014b) and were deformed and metamorphosed during the 2.47–2.41 Ga Sleafordian Orogeny (Daly et al., 1998; McFarlane, 2006; Dutch et al., 2010; Reid et al., 2014b; Halpin and Reid, 2016).

The tectonic setting of the Gawler Craton between ca. 2.00 Ga and 1.73 Ga was dominantly extensional, with a series of rifting events resulting in basin development and widespread deposition of a number of volcanoclastic sedimentary sequences (Fig. 1a; Payne et al., 2006; Fanning et al., 2007; Hand et al., 2007; Payne et al., 2009; Howard et al., 2011b, c; Szpunar et al., 2011; Reid and Hand, 2012; Lane et al., 2015). Widespread basin development and sedimentation was terminated by the Kimban Orogeny at ca. 1.73–1.69 Ga, which involved the development of crustal-scale shear zones, granitic magmatism and widespread metamorphism (e.g. Vassallo and Wilson, 2002; Fanning et al., 2007; Hand et al., 2007; Dutch et al., 2008; Payne et al., 2008; Dutch et al., 2010; Howard et al., 2011c; Morrissey et al., 2016b). Localised clastic basins continued to form within the Kimban orogen (Howard et al., 2011a, b), and more widely an extensive rift basin system developed within the SAC between 1.72 Ga and 1.64 Ga (Conor and Preiss, 2008; Stevens et al., 2008). The Kimban Orogeny was followed by extensive magmatic activity across the Gawler Craton, with the formation of the ca. 1.69–1.67 Ga Tunkillia Suite (Hand et al., 2007; Payne et al., 2010), the ca. 1.62 Ga St Peter Suite (Swain et al., 2008), the voluminous ca. 1.59 Ga Gawler Range Volcanics and the 1.60–1.57 Ga Hiltaba Suite granites (Fanning et al., 1988; Daly et al., 1998; Hand et al., 2007) and the volumetrically minor ca. 1.50 Ga Spilsby Suite in the southern Gawler Craton (Fanning et al., 2007; Jagodzinski et al., 2007). Magmatism at ca. 1.58 Ga was accompanied by widespread, high-grade metamorphism in the northern and southeastern Gawler Craton (Cutts et al., 2011; Forbes et al., 2012; Morrissey et al., 2013), and was part of a widespread event that also affected much of the southeastern NAC (e.g. Boger and Hansen, 2004; Rubenach et al., 2008; Anderson et al., 2013; Morrissey et al., 2014). ^{40}Ar–^{39}Ar and monazite ages from crustal-scale shear zones in the northern and western Gawler Craton suggest that they were reactivated at 1.45–1.40 Ga (Swain et al., 2005b; Fraser and Lyons, 2006). Regional cooling of the craton occurred by 1.40–1.30 Ga (Webb et al., 1986; Hall et al., 2018).

2.3. Northern Gawler Craton

The northern Gawler Craton is very poorly exposed and many of the geological constraints are inferred from geophysics and mineral

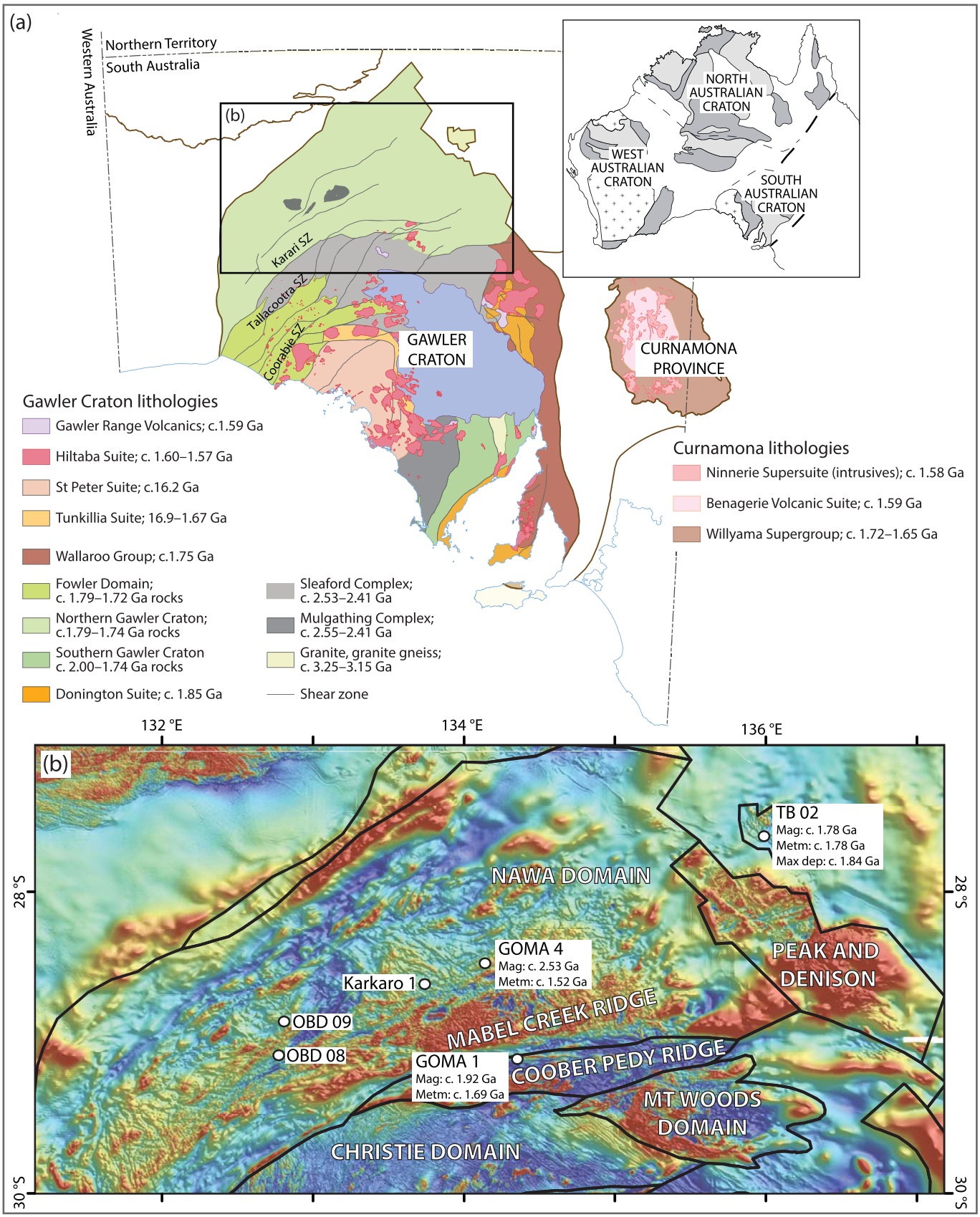

Figure 1. (a) Interpreted simplified solid geology map of the Gawler Craton, after Reid et al. (2014a). Inset is the Gawler Craton in the context of Proterozoic Australia. (b) TMI RTP image of the northern Gawler Craton, showing major geophysically defined domains. Geochronological data from drill holes of interest are from Reid et al. (2014a, 2017).

and petroleum exploration drill holes that intersect basement. The northern Gawler Craton comprises four geophysically defined domains, the Peak and Denison Inlier, the Mount Woods Domain, Coober Pedy Ridge and the Nawa Domain (Fig. 1b). These domains are separated from the Mulgathing Complex in the central Gawler Craton by the crustal-scale Karari Shear Zone (Fig. 1).

In the Peak and Denison Inlier (Fig. 1), migmatitic metasedimentary rocks intersected in drill hole TB 02 have maximum depositional ages of ca. 1.84 Ga and were metamorphosed to upper amphibolite facies at ca. 1.78 Ga (Reid et al., 2017). Metamorphism was synchronous with bimodal magmatism (Reid et al., 2017) and deposition of the protoliths to the Peake Metamorphics and interlayered ca. 1.79–1.77 Ga Tidnamurkuna Volcanics (Fanning et al., 2007). The detrital zircon signature in the migmatitic metasedimentary rocks and timing of ca. 1.78 Ga magmatism and metamorphism are similar to rocks in the Aileron Province of the NAC (Reid et al., 2017). The Peak and Denison rocks were intruded by ca. 1.56–1.53 Ga granites (Fanning et al., 2007).

The protoliths to metasedimentary rocks in the Mount Woods Domain in the north-eastern Gawler Craton (Fig. 1b) have maximum depositional ages of ca. 1.75 Ga (Jagodzinski et al., 2007), and were metamorphosed at ca. 1.73 Ga and 1.61–1.57 Ga (Fanning et al., 1988; Forbes et al., 2011). The Coober Pedy Ridge region occurs to the northwest of Mount Woods and is bounded by splays of the Karari Shear Zone (Fig. 1). The oldest observed rock in the Coober Pedy Ridge region is a 1914 ± 8 Ma granite gneiss intersected in drill hole GOMA DH1 that records high temperature metamorphism at ca. 1.69 Ga (Reid et al., 2014a). Iron-rich metasedimentary rocks overlie the ca. 1.92 Ga basement and were metamorphosed at conditions of 6.5 kbar and ~925 °C at ca. 1.58 Ga (Cutts et al., 2011). The Mount Woods and Coober Pedy Ridge regions were intruded by mafic and felsic magmatic rocks at ca. 1.58 Ga (Fanning et al., 2007).

The Nawa Domain is the northernmost domain of the Gawler Craton and is almost entirely under cover (Fig. 1). As a result, the basement geology is inferred from sparse drill holes and geophysics. Drill hole GOMA DH4 intersected orthogneiss with a magmatic crystallisation age of 2526 ± 7 Ma, suggesting that the northern Gawler Craton is underlain by basement equivalent to the Mulgathing Complex (Reid et al., 2014a). Other drill holes have intersected orthogneisses with crystallisation ages between 1.78–1.75 Ga (Howard et al., 2011c), and metasedimentary rocks deposited between 1.74 Ga and 1.72 Ga (Payne et al., 2006). The protoliths to the metasedimentary rocks are interpreted to be sourced from the Arunta region of the NAC (Payne et al., 2006). Magnetic data from the northern Gawler Craton shows a northeast-trending structural grain that is interpreted to reflect the effects of the ca. 1.73–1.69 Ga Kimban Orogeny (Payne et al., 2008; Howard et al., 2011c; Reid et al., 2014a). In the southern Nawa Domain (Mabel Creek Ridge; Fig. 1), the Kimban-aged structural fabrics underwent extensive high-grade reworking and high-temperature to ultra-high-temperature metamorphism at ca. 1.60–1.55 Ga (Payne et al., 2008; Cutts et al., 2011). Migmatitic orthogneiss in drill hole GOMA DH4 yields a 1521 ± 19 Ma metamorphic zircon age, interpreted to date migmatisation in that sample (Reid et al., 2014a). This age is younger than metamorphic zircon and monazite ages elsewhere in the northern Gawler Craton, and the significance of this age is unclear.

The crustal-scale Karari, Tallacootra and Coorabie Shear Zones in the western and northern Gawler Craton (Fig. 1) yield ca. 1.45 Ga ^{40}Ar–^{39}Ar and monazite ages, thought to reflect reactivation at greenschist to amphibolite facies conditions (Swain et al., 2005b; Fraser and Lyons, 2006; Fraser et al., 2012). These shear zones form part of a craton-scale, northeast-trending fault system that was likely to have been active during the Paleoproterozoic and reactivated in the Mesoproterozoic. The Karari and Coorabie Shear zones show sinistral strike-slip movement, whereas the Tallacootra shear zone shows dextral transport as well as east side-up dip-slip movement. All three are interpreted to be part of a large, transpressional system (Swain et al., 2005b; Thomas et al., 2008). However, it is difficult to determine how much of the movement on these structures reflects Paleoproterozoic/early Mesoproterozoic tectonism or reactivation of older structures at ca. 1.45 Ga.

3. Methods and sample descriptions

Basement rocks in the northern Gawler Craton are not exposed, so the samples in this study were taken from diamond drill holes that were drilled as part of regional mineral exploration programs. Data from three drill holes are presented in this study (Table 1). Drill holes OBD 08 and Karkaro 1 intersect unfoliated granite (Fig. 2a,b). The granite in OBD 08 is medium-grained and contains K-feldspar, plagioclase, quartz and minor biotite. The K-feldspar in samples from OBD 08 is unaltered, but the plagioclase has been altered and hematite stained (Figs. 2a and 3b). Samples 1643401 and 2131380 come from intervals 3 m apart within the same lithology and were used for monazite and zircon geochronology, respectively. Drill hole Karkaro 1 intersects granite with coarse- and fine-grained phases. The two phases are mineralogically identical and contain K-feldspar phenocrysts, plagioclase, quartz and minor biotite. As in OBD 08, plagioclase has been altered (Fig. 3c). The granite in Karkaro 1 was dated using monazite geochronology as the zircon grains were metamict and unsuitable for analysis.

Drill hole OBD 09 intersected strongly foliated garnet–biotite-bearing gneiss that displays evidence for partial melting (Fig. 2c–f). These samples contain garnet, biotite, plagioclase, K-feldspar, quartz, minor pyrite and amorphous Mg-rich clay interpreted to reflect the former presence of cordierite. Monazite geochronology

Table 1
Sample locations and summary. Ages given are LA-ICP-MS U–Pb monazite (mnz) and zircon (zr).

Drill hole					Sample			
Name	No.	(GDA94)	Easting	Northing	Number	Interval (m)	Age (Ma)	Lithology
OBD 08	1577	Z 53	286,298	6,788,087	1643401	180.00–180.40	1458 ± 9 (mnz)	Granite
					2131380	183.00–184.00	1463 ± 15 (zr)	Granite
Karkaro 1	3552	Z 53	380,270	6,835,938	637614	477.39–477.57	1442 ± 9 (mnz)	Fine-grained granite
					637615	479.70–480.01	1463 ± 8 (mnz)	Coarse-grained granite
OBD 09	1592	Z 53	293,375	6,809,107	1643403	389.30–389.80	–	Migmatitic gt–cd–bi gneiss
					2163654A	390.27–390.38	–	Migmatitic gt–cd–bi gneiss
					2163654B	390.38–390.47	–	Gt–cd-bearing leucosome
					660842	391.95–392.25	–	Migmatitic gt–bi gneiss
					2163655	400.31–400.41	–	Migmatitic gt–bi gneiss
					1643405	396.10–396.50	1444 ± 10 (mnz)	Migmatitic gt–bi gneiss

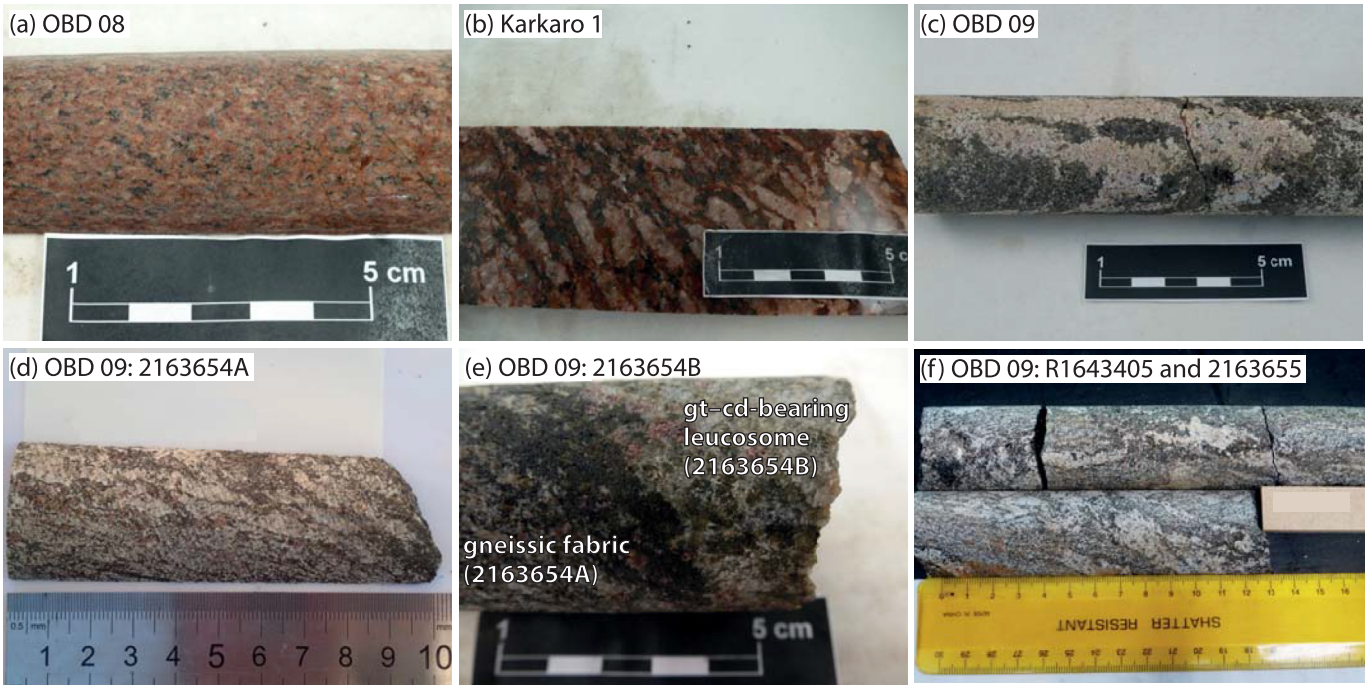

Figure 2. Photographs of lithologies from core yielding ca. 1.45 Ga ages. (a) Medium-grained phase of granite in drill hole OBD 08 (sample 1643401). (b) Coarse-grained phase of Karkaro granite in drill hole Karkaro 1 (sample 637615). (c) Cross cutting leucosomes in drill hole OBD 09, bounded by garnet–biotite melanosomes 1 cm in width. (d) Garnet–biotite gneiss in drill hole OBD 09 (sample 2163654A). (e) Cross cutting garnet–cordierite-bearing leucosome in drill hole OBD 09 (sample 2163654B). (f) Garnet–biotite gneiss in drill hole OBD 09, used for phase diagram calculation (sample 2163655) and geochronology (sample R1643405).

and phase diagram analysis is presented from drill hole OBD 09 to constrain the timing and conditions of metamorphism.

3.1. LA-ICP-MS geochronology

3.1.1. LA-ICP-MS zircon geochronology

Zircon grains in sample OBD 08 were separated from crushed rock using a combination of hand panning, magnetic separation and heavy liquids techniques, and heat treated at 900 °C for 48 h. Zircon yield from this sample was very low so all zircon grains from this sample were picked and mounted in epoxy resin. Cathodoluminescence (CL) imagery of zircon was collected using a FEI Quanta600 Scanning Electron Microscope equipped with a Gatan CL detector at Adelaide Microscopy, the University of Adelaide, Australia.

U–Pb zircon geochronology was done by Laser-Ablation Inductively-Coupled Plasma-Mass Spectrometry (LA-ICP-MS) at Adelaide Microscopy, the University of Adelaide, Australia, using an ASI M–50 193-nm excimer laser coupled to an Agilent 7700s Quadrupole ICP-MS. Each analysis involved simultaneous measurement on masses ^{202}Hg, ^{204}Pb, ^{206}Pb, ^{207}Pb, ^{208}Pb, ^{232}Th and ^{238}U for dwell times of 20, 20, 30, 60, 20, 20 and 30 ms, respectively. Zircons were ablated with a frequency of 5 Hz, intensity of approximately 2–3 J cm^{-2} and a spot size of 30 μm. The acquisition time of each analysis was 100 s, inclusive of five pre-ablation laser pulses to remove surficial contamination, 50 s of background measurement and 50 s of ablation.

Iolite (v. 3.0) was used to reduce raw data including corrections for baseline, instrumental drift, mass bias and down-hole fractionation (Paton et al., 2011). Data were corrected using the zircon standard GJ-1 (TIMS normalisation data: ^{207}Pb/^{206}Pb = 608.3 Ma, ^{206}Pb/^{238}U = 600.7 Ma, ^{207}Pb/^{235}U = 602.2 Ma; Jackson et al., 2004). Data accuracy was monitored using repeated analysis of secondary standards Plešovice (^{206}Pb/^{238}U = 337.13 ± 0.37 Ma; Slama et al., 2008) and 91500 (^{207}Pb/^{206}Pb = 1065 Ma; Wiedenbeck et al., 1995). Throughout the analytical session, Plešovice and 91500 yielded respective weighted mean ages of ^{206}Pb/^{238}U = 336.9 ± 3.0 Ma (n = 6; MSWD = 0.93), and ^{207}Pb/^{206}Pb = 1067 ± 28 Ma (n = 7; MSWD = 0.94), respectively. Common Pb corrections were not performed due to isobaric interference of ^{204}Hg on the ^{204}Pb isotope peak. Instead, analyses were discarded where significant levels of ^{204}Pb (^{204}Pb/^{206}Pb > 0.0005) were observed during analysis. U–Pb data are presented in Appendix 1. Uncertainties on spot analyses and weighted average ages are given at the 2σ level.

3.1.2. LA-ICP-MS monazite geochronology

Analytical techniques for in situ U–Pb monazite dating follow the method of Payne et al. (2008). Monazite grains were imaged prior to analysis using a back-scattered electron detector on a Phillips XL30 SEM at the University of Adelaide, Australia. U–Pb isotopic analyses were collected using a New Wave 213 nm Nd–YAG laser in a He ablation atmosphere, coupled to an Agilent 7500cs/7500s ICP-MS at the University of Adelaide, Australia. Monazites were ablated using a spot size of 15 μm. The total acquisition time of each analysis was 100 s. This included 40 s of background measurement, 10 s of the laser firing with the shutter closed to allow for beam stabilisation, and 40s of sample ablation. Isotopes measured were ^{204}Pb, ^{206}Pb, ^{207}Pb and ^{238}U for dwell times of 10, 15, 30 and 15 ms, respectively.

Monazite data were reduced using Glitter software (Jackson et al., 2004). Element fractionation and mass bias was corrected using the MAdel monazite standard (TIMS normalisation data: ^{207}Pb/^{206}Pb = 490.7 Ma, ^{206}Pb/^{238}U = 514.8 Ma and ^{207}Pb/^{235}U = 510.4 Ma; Payne et al., 2008). Accuracy was monitored with the 44069 monazite standard (TIMS normalisation data: ^{207}Pb/^{206}Pb = 425.3 ± 1.1 Ma, ^{206}Pb/^{238}U = 424.86 ± 0.36 Ma and ^{207}Pb/^{235}U = 424.89 ± 0.35 Ma; Aleinikoff et al., 2006) and an in-house monazite standard 94-222/Bruna-NW (ca. 450 Ma; Payne et al., 2008). Throughout the study, 16 analyses of 44069 yielded

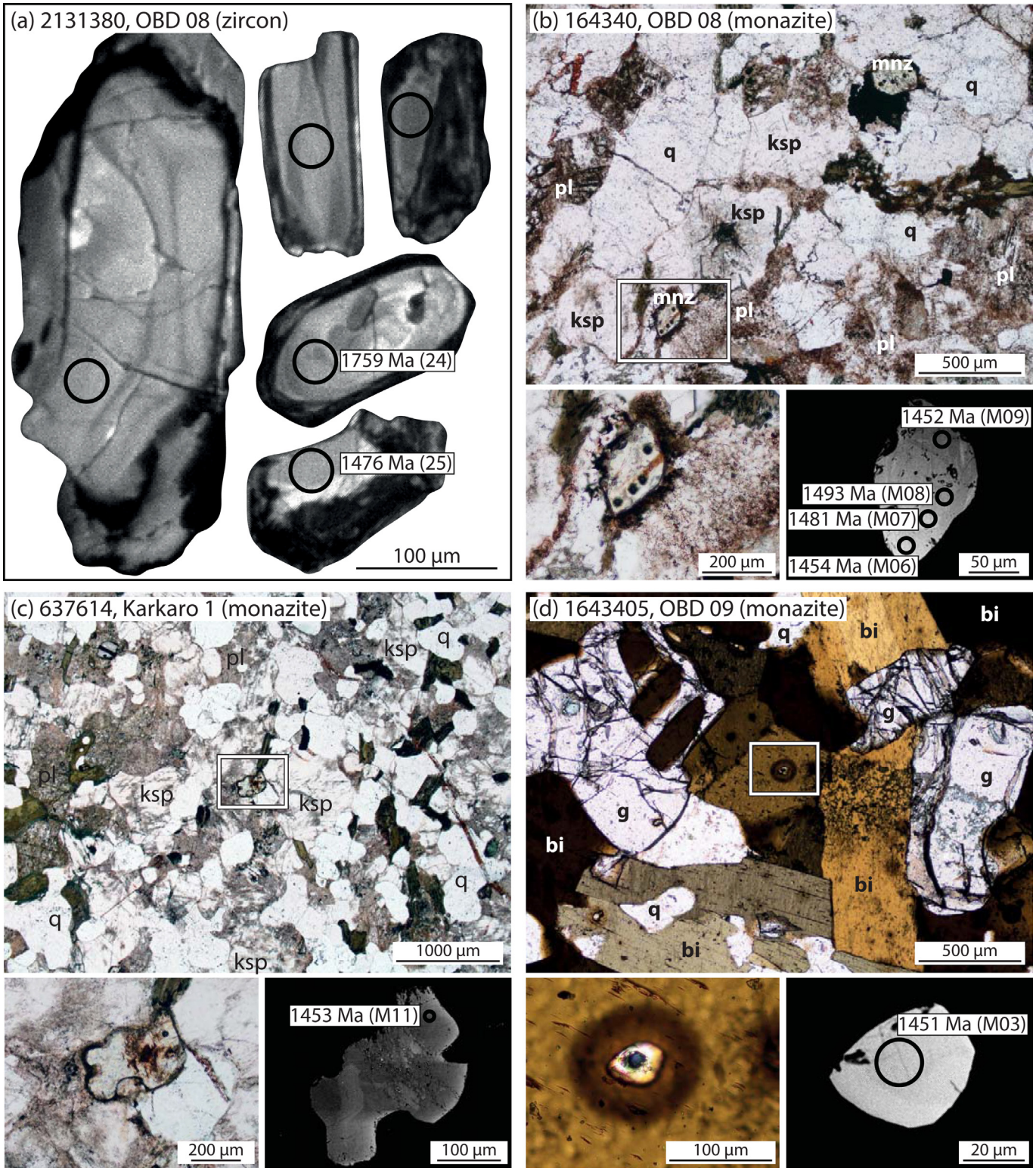

Figure 3. Images of zircon and monazite used for LA-ICP-MS geochronology. (a) Cathodoluminescence images of zircon from sample 2131380 (granite; OBD 08). Spot ages are the $^{207}Pb/^{206}Pb$ age. (b–d) Images of representative monazite grains from samples 164340 (granite; OBD 08), 637614 (fine-grained granite; Karkaro 1) and 1643405 (garnet–biotite gneiss; OBD 09) showing microstructural location and BSE zoning.

weighted mean ages of $^{207}Pb/^{206}Pb = 418 \pm 13$ Ma (MSWD = 0.84), $^{206}Pb/^{238}Pb = 424 \pm 3$ Ma (MSWD = 1.03) and $^{207}Pb/^{235}Pb = 423 \pm 3$ Ma (MSWD = 1.20) and 23 analyses of 94-222/Bruna-NW yielded weighted mean ages of $^{207}Pb/^{206}Pb = 441 \pm 13$ Ma (MSWD = 0.77), $^{206}Pb/^{238}Pb = 452 \pm 3$ Ma (MSWD = 1.00) and $^{207}Pb/^{235}Pb = 450 \pm 3$ Ma (MSWD = 0.76). Analyses were discarded where significant levels of ^{204}Pb ($^{204}Pb/^{206}Pb > 0.0005$) were observed during analysis. U–Pb monazite data are presented in Appendix 2. Uncertainties on individual spot ages are given at the 1σ level, uncertainties on weighted average ages are 2σ.

3.2. Whole rock geochemistry and isotopic data

Whole rock geochemical compositions of magmatic rocks were obtained from Amdel Limited, South Australia. For the acquisition of major elements, a sub-sample of 0.1 g of analytical pulp was fused with lithium metaborate followed by dissolution to give a total solution, which was run on an ICP-OES. Trace and rare earth element data were acquired from the digestion of 0.2 g sub-sample of analytical pulp in HF and multi acid digest, the solution was then run on an ICP-MS and an ICP-OES. Whole rock geochemical data are presented in Table 2.

Table 2
Whole rock geochemistry (major elements in wt.%, trace elements in ppm).

	Karkaro 1 637614	Karkaro 1 637615	OBD 08 1643401	OBD 09 2163654A	OBD 09 2163655
SiO_2	72	72	72	54.77	56.84
TiO_2	0.2	0.2	0.3	0.98	1.04
Al_2O_3	14	14	13	18.79	17.41
Fe_2O_3	2.3	1.7	1.9	9.91	11.42
MnO	0.02	0.02	0.02	0.31	0.33
MgO	0.5	0.4	0.8	3.79	3.60
CaO	0.4	0.5	0.3	0.73	1.76
Na_2O	3.1	2.9	2.6	1.57	2.05
K_2O	6.3	6.7	7.0	8.91	5.34
P_2O_5	0.1	0.1	0.1	0.11	0.18
LOI	n.a.	n.a.	1	2.08	1.30
La	105	96	160	25	27
Ce	185	175	300	63	58
Pr	20	19	33	n.a	n.a.
Nd	64	60	105	n.a	n.a.
Sm	13	11	15	n.a	n.a.
Eu	1.4	1.2	2.4	n.a	n.a.
Gd	9	8	9	n.a	n.a.
Tb	1.4	1.2	1.3	n.a	n.a.
Dy	7.5	6	6	n.a	n.a.
Ho	1.4	1	0.9	n.a	n.a.
Er	3.5	2.4	2.5	n.a	n.a.
Tm	0.5	0.3	0.3	n.a	n.a.
Yb	2.7	1.4	1.9	n.a	n.a.
Lu	0.4	0.2	0.3	n.a	n.a.
Ag	b.d.	b.d.	0.3	n.a	n.a.
As	0.5	2	1.5	n.a	n.a.
Ba	800	430	580	864	781
Be	3	4.5	n.a.	n.a	n.a.
Bi	b.d.	b.d.	0.1	n.a	n.a.
Cd	0.4	0.2	b.d.	n.a	n.a.
Co	32	23	70	28	39
Cr	b.d.	b.d.	b.d.	85	98
Cs	1.5	2.2	1.8	n.a	n.a.
Cu	1.5	2.5	5	16	78
Ga	25	26	17	26.7	25.6
Hf	7	6	n.a.	n.a	n.a.
In	b.d.	b.d.	b.d.	n.a	n.a.
Mo	1.2	0.8	1.1	n.a	n.a.
Nb	20	20	18	19.5	18.4
Ni	b.d.	b.d.	b.d.	54	75
Pb	46	52	47	23	<1
Rb	310	320	270	424.1	331.3
Sb	b.d.	b.d.	b.d.	n.a	n.a.
Sc	b.d.	b.d.	b.d.	16	13
Se	1	1	b.d.	n.a	n.a.
Sn	b.d.	b.d.	n.a.	n.a	n.a.
Sr	76	62	175	81	88
Ta	b.d.	b.d.	n.a.	n.a	n.a.
Te	b.d.	b.d.	0.2	n.a	n.a.
Th	60	94	145	25.2	23.0
Tl	1.8	2	1.7	n.a	n.a.
U	7	9	4	b.d.	b.d.
V	b.d.	b.d.	b.d.	160	152
W	280	185	n.a.	n.a	n.a.
Y	32	25	32	17.5	22.7
Zn	29	30	27	159	156
Zr	200	170	260	195	201

Whole rock chemical compositions for the construction of metamorphic phase diagrams for two samples from the OBD 09 drill hole were obtained by XRF at Franklin and Marshall College, Pennsylvania following the method of Boyd and Mertzman (1987). The drill holes are narrow (~5 cm in diameter) so geochemistry was obtained from the thin section blocks. Major elements were analysed by mixing a 0.4 g portion of the powdered sample with 3.6 g of lithium tetraborate for measurement of the major elements by XRF. Trace elements were analysed by mixing 7 g of whole rock powder with 1.4 g of high purity Copolywax powder and measured by XRF. The whole rock composition for each sample is given in Table 2.

Sm–Nd isotope analyses were undertaken at the University of Adelaide, Australia, following the technique of Wade et al. (2005). Samples were spiked with a $^{150}Nd/^{147}Sm$ solution then evaporated in HF. The samples were then digested in HF in sealed Teflon bombs at 190 °C for 5 days then evaporated, with HNO_3 added shortly before samples were completely dry. Samples were then heated for 2 days in 6 M HCl. Rare earth elements (REE) were separated in Biorad Polyprep columns loaded with Biorad AG50W X8 (200–400 mesh) resin, and were further separated in HDEHP-impregnated Teflon-powder columns to isolate Sm and Nd. Nd was analysed using a Finnigan MAT 262 Thermal Ionisation Mass Spectrometer (TIMS) and Sm was analysed using a Finnigan MAT 261 TIMS. The La Jolla and JNdi-1 standards give long term running averages of 0.511834 ± 0.000018 (2σ, $n = 96$) and 0.512092 ± 0.000016 (2σ, $n = 164$), respectively.

3.3. Metamorphic phase equilibria

Phase equilibria models for two samples of garnet-bearing gneiss from drill hole OBD 09 were calculated using THERMOCALC v3.40, using the internally consistent dataset, ds62, of Holland and Powell (2011) and the activity–composition (a–x) models re-parameterised for metapelitic rocks in the system MnNCKFMASHTO ($MnO–Na_2O–CaO–K_2O–FeO–MgO–Al_2O_3–SiO_2–H_2O–TiO_2–Fe_2O_3$) (Powell et al., 2014; White et al., 2014a, b).

It has been widely recognised that variations in the H_2O and Fe_2O_3 components of the bulk composition may affect the stability of phase assemblages in P–T space (e.g. White et al., 2000; Johnson and White, 2011). Determination of Fe_2O_3 by titration may overestimate the amount of Fe_2O_3 in the whole rock geochemistry due to low-T oxidation during weathering, or oxidation during sample preparation for geochemical analysis (e.g. Johnson and White, 2011; Lo Pò and Braga, 2014; Kelsey and Hand, 2015). The samples contain rare pyrite, suggesting a relatively reduced composition, so approximately 5% of total iron was assumed to be Fe^{3+}. Although no Fe-oxides are present in the samples, the pseudosections were calculated in an Fe_2O_3-bearing system to reflect that there is likely to be a small amount of Fe_2O_3 present in natural rocks, which can modify the stability of silicate minerals such as biotite (White et al., 2002).

The samples in this study are migmatitic and are likely to have lost melt (Fig. 2). The measured LOI may only provide a maximum value for the amount of H_2O at peak conditions due to hydration of the sample during low-temperature retrogression and weathering, as well as the presence of other volatiles such as CO_2, F and Cl. The H_2O contents for each sample relating to the peak conditions were assessed using T–M_{H_2O} sections, presented in Appendix 3. The main effect of decreasing the H_2O content of the bulk composition in these samples is to elevate the solidus and decrease the stability of cordierite, whereas a high H_2O content stabilises sillimanite. The H_2O content of each sample was selected so that the peak assemblage is bounded to lower temperatures by the elevated solidus,

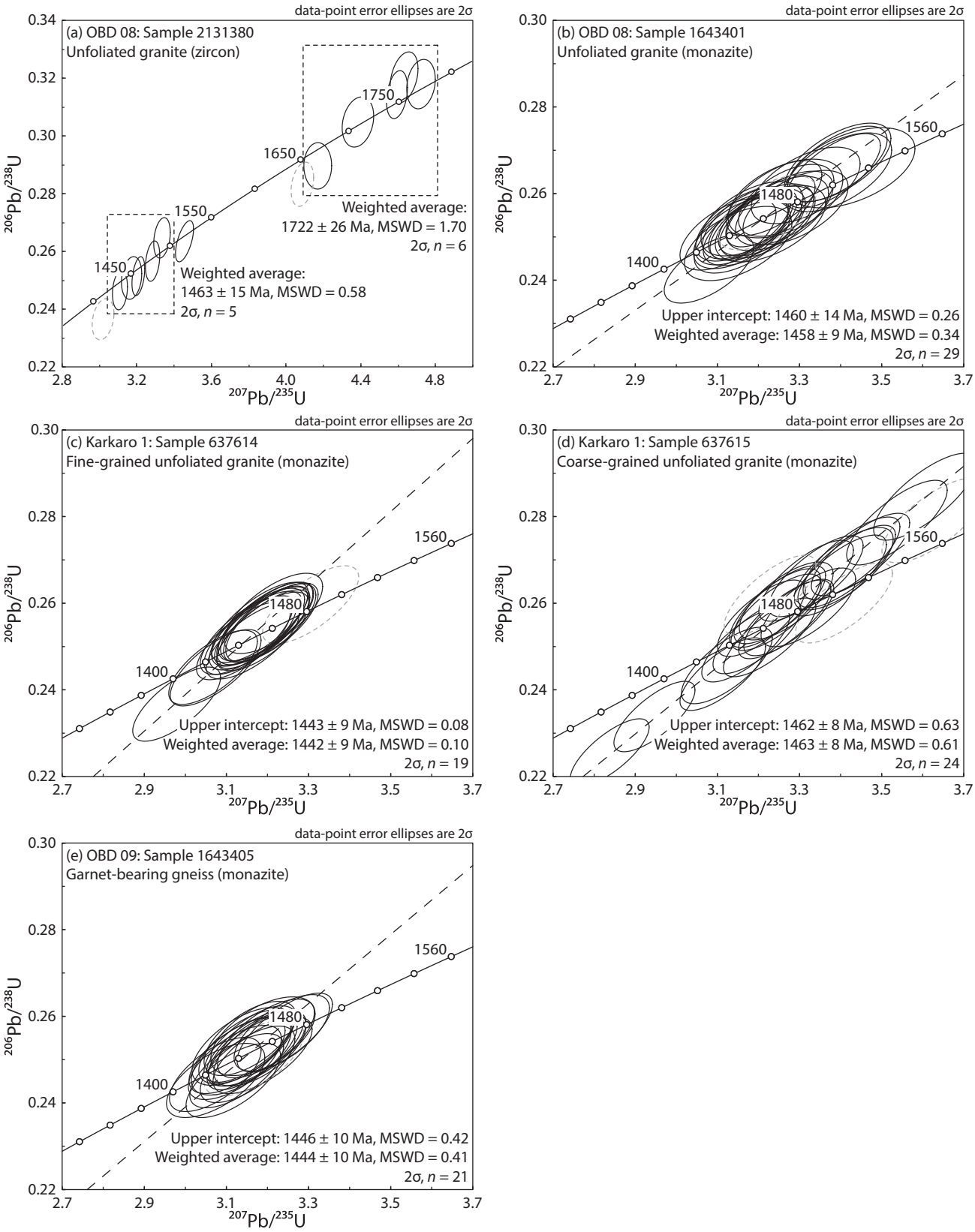

Figure 4. LA-ICP-MS zircon (a) and monazite (b–e) U–Pb geochronology. The weighted average ages given are the $^{207}Pb/^{206}Pb$ ages. Analyses denoted by dashed, grey ellipses are excluded from the calculation of weighted averages and intercept ages. (a) Sample 2131380. (b) Sample 1643401. (c) Sample 637614. (d) Sample 637615. (e) Sample 1643405.

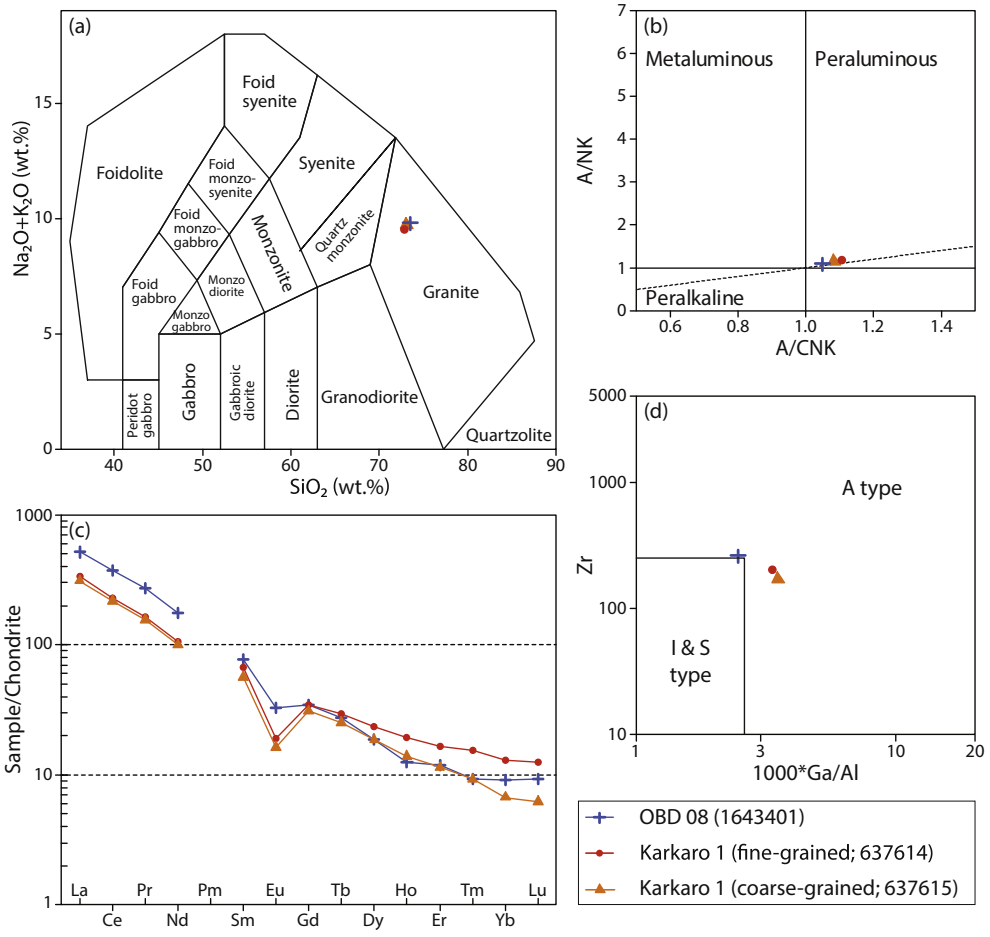

Figure 5. Geochemical plots for magmatic samples. (a) TAS plot (Middlemost, 1994). (b) A/CNK–A/NK plot. (c) REE chondrite spider plot (Boynton, 1984). (d) Zr–Ga/Al (Whalen et al., 1987).

reflecting the conditions where the assemblage would have been in equilibrium with the last vestiges of melt (White et al., 2004; Diener et al., 2008).

4. Results

4.1. Zircon U–Pb geochronology

4.1.1. OBD 08: granite, sample 2131380

The sample volume available for zircon geochronology was small and therefore zircon yield in this sample was low. Zircon grains are light to dark brown in colour, predominantly 150–200 μm in length and have aspect ratios of 1:1.2 to 1:2 (Fig. 3a). They commonly display a bright, weakly zoned to unzoned core surrounded by dark, weakly zoned rims (Fig. 3a). Rare, dark grains with no bright core also occur and are interpreted to be equivalent in morphology to the dark rims. These dark rims and grains were highly discordant and so did not give easily interpreted age information. All analyses come from bright core domains (Fig. 3a).

Fourteen analyses were collected from 14 zircon grains from this sample. An additional 10 spots were analysed on dark rims and grains that were too metamict to yield meaningful results. Three analyses are more than 5% discordant (one not shown) and were excluded from further interpretation. The remaining 11 analyses define two distinct populations (Fig. 4a). The oldest population yields a range of $^{207}Pb/^{206}Pb$ ages from 1759 Ma to 1692 Ma with a $^{207}Pb/^{206}Pb$ weighted average age of 1722 ± 26 Ma (n = 6; MSWD = 1.70). The analyses from the youngest population range in age from 1527 Ma to 1448 Ma. The $^{207}Pb/^{206}Pb$ weighted average age of all six analyses in the youngest population is 1476 ± 31 Ma with a high MSWD of 3.0, suggesting the analyses do not form a single population. Exclusion of the oldest analysis decreases the MSWD and gives a weighted average age of 1463 ± 15 (n = 5; MSWD = 0.58).

4.2. Monazite U–Pb geochronology

4.2.1. OBD 08: granite, sample 1643401

Monazite grains in this sample are 60–200 μm in diameter and are located within feldspar and quartz grains as well as along grain boundaries (Fig. 3b). Twenty-nine analyses were collected from this sample. One analysis was excluded on the basis of high $^{204}Pb/^{206}Pb$ ratios. A concordia plot of the remaining 28 analyses yields an upper intercept age of 1460 ± 14 Ma (MSWD = 0.26; Fig. 4b). The $^{207}Pb/^{206}Pb$ weighted average age for this sample is 1458 ± 9 Ma (n = 29; MSWD = 0.34).

4.2.2. Karkaro 1: fine-grained granite, sample 637614

Zircon grains from the Karkaro 1 samples were metamict and unsuitable for analysis, so monazite geochronology was undertaken. Monazite grains in this sample are 40–100 μm in diameter and are located within feldspar and quartz grains as well as along grain boundaries (Fig. 3c). Twenty analyses were collected from this sample. One analysis was excluded using linearised probability plots. A concordia plot of the remaining 19 analyses yields an upper intercept of

Table 3
Sm–Nd isotope data from granitic rocks.

Drill hole	Sample	Rock type	Sm (ppm)	Nd (ppm)	$^{147}Sm/^{144}Nd$	$^{143}Nd/^{144}Nd$	2σ	$\varepsilon_{Nd}(0)$	$\varepsilon_{Nd}(t)$	Age (Ma)
OBD 08	1643401	Granite	11.2	81.0	0.0834	0.511162	9	−28.8	−7.8	1450
Karkaro 1	367614	Granite	13.0	68.7	0.1143	0.511138	10	−29.3	−14.0	1450
Karkaro 1	367615	Granite	9.1	52.0	0.1056	0.511325	10	−25.6	−8.7	1450
OBD 09	660842	Migmatitic gt–bi gneiss	7.5	41.1	0.1147	0.511476	6	−22.6	−7.5	1450
OBD 09	1643403	Migmatitic gt–bi gneiss	9.0	51.9	0.1052	0.511336	12	−25.4	−8.4	1450

Notes: $^{143}Nd/^{144}Nd_{\ CHUR(0)} = 0.512638$, $^{147}Sm/^{144}Nd_{\ CHUR(0)} = 0.1966$.

1443 ± 9 Ma (MSWD = 0.08; Fig. 4c). The $^{207}Pb/^{206}Pb$ weighted average age for this sample is 1442 ± 9 Ma (n = 19; MSWD = 0.10).

4.2.3. Karkaro 1: coarse-grained granite, sample 637615

Monazite grains in this sample are typically 50–150 μm in diameter. Twenty-eight analyses were collected from this sample. Four analyses were excluded from further interpretation using linearised probability plots. A concordia plot of the remaining 24 analyses yields an upper intercept of 1462 ± 8 Ma (MSWD = 0.63; Fig. 4d). The $^{207}Pb/^{206}Pb$ weighted average age for this sample is 1463 ± 8 Ma (n = 24; MSWD = 0.61).

4.2.4. OBD 09: garnet–cordierite–biotite gneiss, sample 1643405

Monazite grains are typically 50–80 μm in diameter and located within feldspar and biotite grains (Fig. 3d). Twenty-two analyses were collected from this sample. One analysis was rejected on the basis of $^{204}Pb/^{206}Pb$ ratios. A concordia plot of the remaining 21 analyses yields an upper intercept age of 1446 ± 10 Ma (MSWD = 0.42; Fig. 4e). The $^{207}Pb/^{206}Pb$ weighted average age for this sample is 1444 ± 10 Ma (n = 21; MSWD = 0.41). The mineral assemblage in this sample suggests that it has a metasedimentary protolith, and therefore the ca. 1.45 Ga monazite age is interpreted to reflect the timing of metamorphism.

4.3. Geochemistry of the high-K granites

The felsic magmatic rocks from drill holes OBD 08 and Karkaro 1 are similar in composition (Fig. 5, Table 2). All samples have high K_2O of 6.3–7 wt.%, high K/Na ratios and are slightly peraluminous. High REE compositions, steep LREE-enriched patterns and high Ga/Al values suggest the samples can be interpreted as "A-type" granites (Fig. 5; Whalen et al., 1987). Sm–Nd isotopic data (initial ε_{Nd} values of −14 to −8.7) suggest the granites were derived predominantly from melting of ancient crust (Table 3). Two samples of metasedimentary rock from OBD 09 have similar ε_{Nd} (1450 Ma) values of −7.5 and −8.4 indicating the crustal source for the granites could be similar to that sampled in OBD 09, but is likely to contain a component of older crustal material as well (Table 3).

4.4. Petrography and pressure–temperature conditions

Two samples of garnet-bearing gneiss from drill hole OBD 09 were selected for metamorphic analysis to obtain basic constraints on the thermal regime operating at ca. 1.45 Ma. The gneissic basement rocks intersected in OBD 09 contain leucosomes that are semi-concordant to discordant to the foliation that are bounded by biotite–garnet melanosomes up to 1 cm in width (Fig. 2c–f). Therefore, the peak assemblages are interpreted to have developed in the presence of melt.

4.4.1. OBD 09: sample 2163654A and B (garnet–biotite gneiss)

Sample 2163654A is a garnet–biotite-bearing gneiss that is cross-cut by garnet–psueodmorphed cordierite-bearing leucosomes (represented by sample 2163654B; Fig. 2d,e). The sample contains garnet, K-feldspar, biotite, plagioclase, cordierite and quartz. The sample has a weak gneissic foliation defined by alternating biotite and K-feldspar-rich layers. Garnet grains are 1.2–3 mm and occur in the biotite-rich layers. Fractures within garnet are filled by fine-grained muscovite (Fig. 6a). Biotite flakes are oriented parallel to the foliation. Plagioclase (200–1000 μm) occurs throughout the sample. K-feldspar (up to 4000 μm) is extremely abundant and occurs as perthite and microcline. K-feldspar porphyroblasts contain inclusions of fine-grained biotite (250–400 μm), fine-grained plagioclase (200 μm) and quartz (Fig. 6a). This sample also contains anhedral domains of an amorphous mineral that is rimmed by intergrown muscovite–chlorite (Fig. 6a). These domains occur throughout the sample, including within the K-feldspar-rich layers, but are the most abundant in the biotite–garnet-bearing layers. These domains are very similar in appearance to euhedral domains of finely intergrown muscovite–chlorite and an amorphous mineral in the cross-cutting leucosome, which are interpreted to be pseudomorphed cordierite (Fig. 6b,c). The cross-cutting leucosome (sample 2163654B) contains coarse-grained, euhedral garnet and quartz porphyroblasts that are up to 5 mm in diameter, as well as unoriented biotite (2 mm in length) and K-feldspar (Fig. 6b,c). Rare pyrite occurs throughout the biotite–garnet gneiss and leucosome.

The field on the P–T pseudosection that best corresponds to the peak mineral assemblage in sample 2163654A contains garnet + plagioclase + K-feldspar + biotite + cordierite + ilmenite + quartz + silicate melt. This field occurs at conditions of 3–6 kbar and 775–820 °C (Fig. 7a). The absence of sillimanite in the rock provides an upper pressure constraint of 5.2–6 kbar whereas the presence of quartz provides an upper temperature constraint of 820 °C. The elevated solidus provides a minimum temperature constraint of 775–795 °C. Cordierite is calculated to be stable throughout the lower-P part of the pseudosection, lending support to the inference that the weathered domains are pseudomorphs after cordierite. Ilmenite is stable throughout the pseudosections but is not present in the rock. However, the modelled modal abundance in the peak field is very small (0.2–0.6 mol%) and its presence in the pseudosection is not interpreted to affect the P–T conditions.

4.4.2. OBD 09: sample 2163655

Sample 2163655 contains a weak gneissic fabric defined by discontinuous quartzofeldspathic segregations that are wrapped by biotite-rich layers (Fig. 2f). The quartzofeldspathic layers are up to 5 mm in width and contain euhedral plagioclase (500–1500 μm), K-feldspar (3000 μm) and quartz. At thin section scale, tabular flakes of biotite (500–2500 μm) are weakly oriented parallel to the gneissic fabric. Abundant euhedral garnet grains (1000–1500 μm in diameter) occur in the biotite-rich layers and commonly contain inclusions of quartz in the cores. K-feldspar porphyroblasts (>5000 μm in length) also occur in the biotite-rich layers and contain inclusions of fine-grained biotite (250–400 μm) that are oriented along feldspar cleavage planes and rare, fine-grained plagioclase and quartz (Fig. 6d). Finer-grained plagioclase and quartz occur within the biotite-rich layers. Extremely rare pyrite

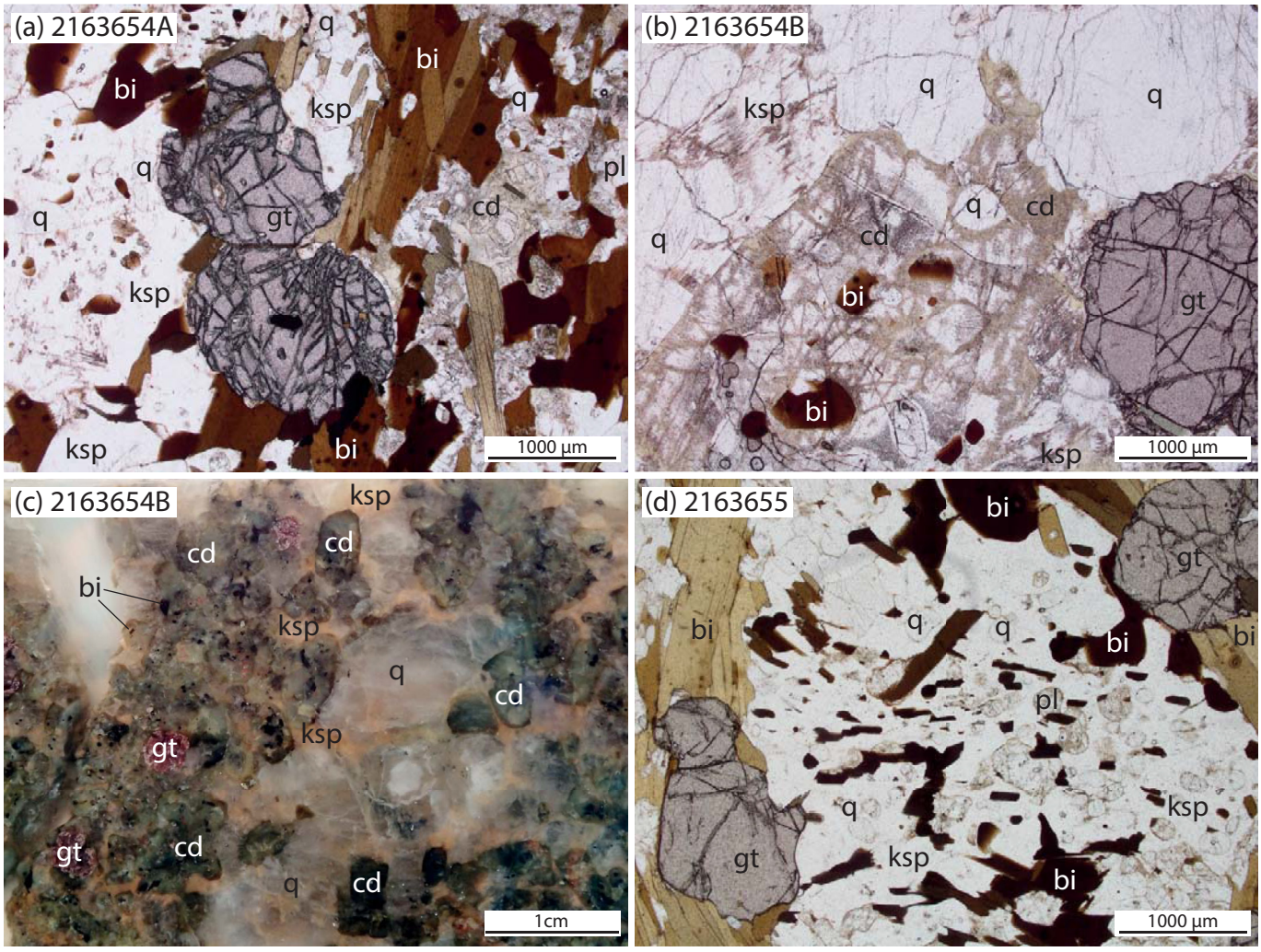

Figure 6. Photomicrographs from drill hole OBD 09. Abbreviations are: bi (biotite), cd (cordierite), gt (garnet), ksp (K-feldspar), pl (plagioclase), q (quartz). (a) Sample 2163654A: garnet–biotite gneiss containing domains of altered cordierite. (b) 2163654B: garnet–cordierite-bearing leucosome. Cordierite has now been replaced but occurs as domains with a different weathering character to the altered K-feldspar. (c) Sample 2163654B: photograph of thick section showing relationships between quartz, K-feldspar, garnet and altered cordierite. The altered cordierite grains occur as euhedral domains that are rimmed by muscovite-chlorite intergrowths. K-feldspar occurs as hematite-stained interstitial grains around quartz and cordierite. (d) Sample 2163655: garnet–biotite gneiss. K-feldspar grains contain inclusions of aligned biotite and plagioclase, which are commonly discordant to the main gneissic fabric.

occurs throughout the sample. This sample contains rare domains of an amorphous mineral that is very similar in appearance to pseudomorphed cordierite in sample 2163654A.

The field on the *P–T* pseudosection that best corresponds to the peak mineral assemblage in sample 2163655 contains garnet + plagioclase + K-feldspar + biotite + cordierite + ilmenite + quartz + silicate melt. This field occurs at conditions of 3–5.4 kbar and 775–815 °C (Fig. 7b). The absence of sillimanite in the rock provides an upper pressure constraint of 5–5.4 kbar and the elevated solidus provides a minimum temperature constraint of 775–790 °C. The interpretation of peak cordierite in this sample is more ambiguous than in sample 2163654A as domains that may have been pseudomorphed cordierite are rare. However, the peak field is not predicted to contain large volumes of cordierite, with ~2 mol% modelled to occur in the higher-*P*, lower-*T* corner of the peak field. This suggests that peak conditions were in the higher-*P* part of the field. As in sample 2163654A, ilmenite is not present in rock but occurs in the peak field in modally small amounts (0.4–0.6 mol%).

5. Discussion

5.1. Thermal character and footprint of ca. 1.45 Ga metamorphism

The sample of garnet-bearing migmatitic gneiss from drill hole OBD 09 gives a monazite age of 1444 ± 10 Ma (Fig. 4e), interpreted to date the timing of granulite facies metamorphism. Samples 2163654A and 2163655 are both from drill hole OBD 09 and therefore their calculated *P–T* pseudosections can be overlain to provide tighter constraints on the metamorphic conditions. These suggest that peak conditions involved temperatures of 775–815 °C and pressures of 3.2–5.4 kbar (Fig. 7). The higher-*P* part of this range is most consistent with the paucity of altered cordierite in sample 2163655.

The three granitic samples (from drill holes OBD 08 and Karkaro 1) in this study give monazite ages between 1463 ± 8 Ma and 1442 ± 9 Ma (Fig. 4b–d). Zircon geochronology was only possible from sample 2131380 from OBD 08, as the zircon grains from the Karkaro 1 samples were metamict and could not be analysed to

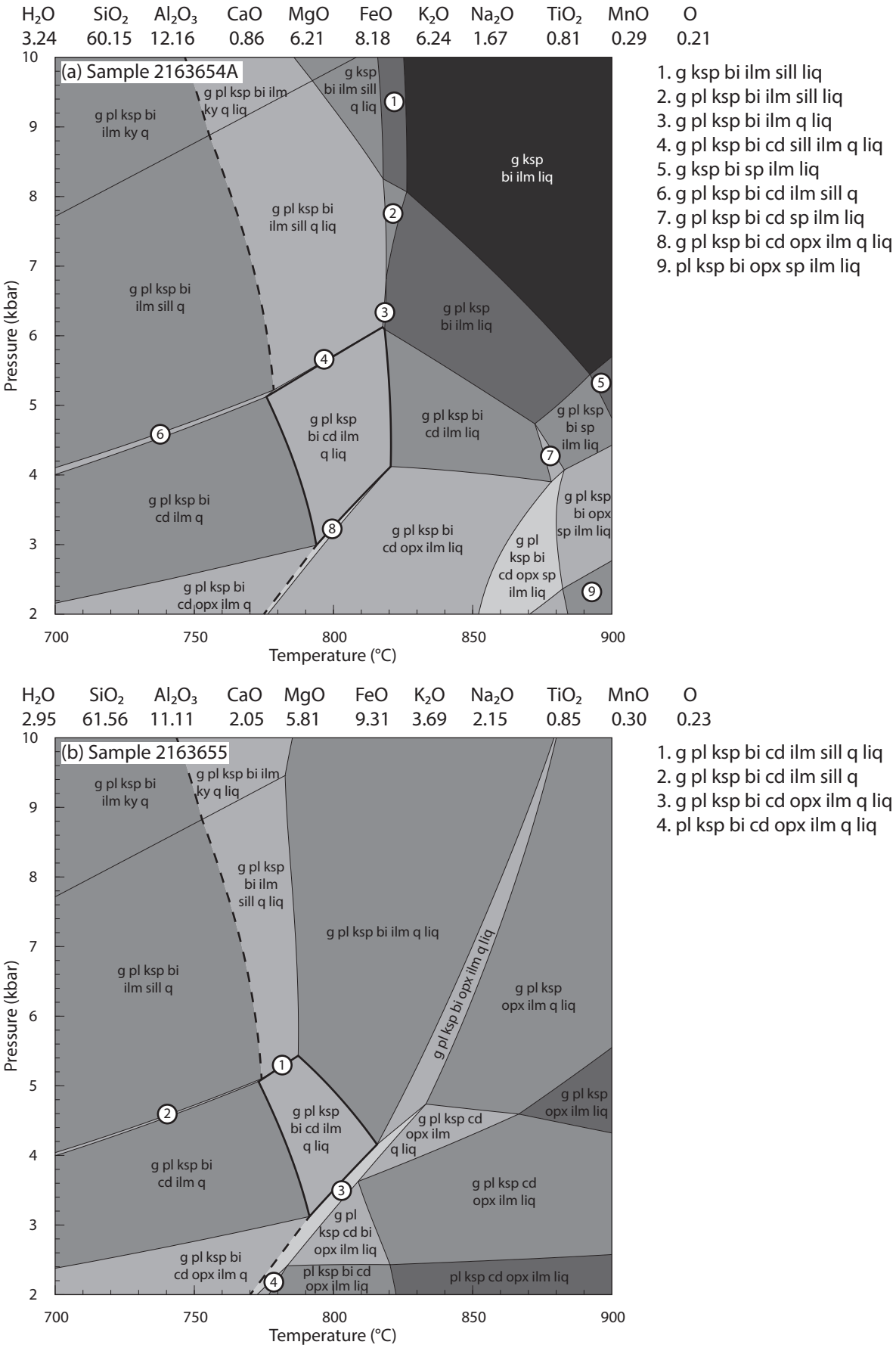

Figure 7. Calculated *P*–*T* pseudosections for two samples of garnet-bearing gneiss from drill hole OBD 09. The bulk rock composition in mol% is given above the pseudosection. The bold dashed line is the solidus. The interpreted peak field for each sample is outlined in bold. (a) Sample 2163654A. (b) Sample 2163655.

provide meaningful age data. However, the three granitic samples have similar monazite ages, geochemistry and mineralogy and are likely to be temporally equivalent (Figs. 2–5). The zircon ages from OBD 08 come from bright, weakly zoned cores and define two populations at 1722 ± 26 Ma and 1463 ± 15 Ma (Figs. 3a and 4a). The oldest ages are consistent with the ca. 1.73–1.69 Ga Kimban Orogeny, which is interpreted to have pervasively affected the northern Gawler Craton (e.g. Payne et al., 2008; Armit et al., 2017). The granites are undeformed and do not show any evidence for metamorphism (Figs. 2 and 3), meaning that they are likely to have post-dated the Kimban Orogeny. Therefore, the ca. 1.72 Ga ages are interpreted to be inherited. The younger (1463 ± 15 Ma) age population is within uncertainty of the monazite age of 1458 ± 9 Ma for the same granite. Therefore, it is likely that the ca. 1.45 Ga monazite ages in each of the granitic samples reflects the timing of crystallisation of the granites. The ca. 1.45 Ga granites have similar chemistry to the A-type Hiltaba granites, which were emplaced throughout the central and southern Gawler Craton over a short interval from ca. 1.60 Ga to 1.57 Ga (Hand et al., 2007). The Hiltaba granites are interpreted to form part of a short-lived large igneous province that may have formed in an intracontinental setting (Wade et al., 2012). The ca. 1.45 Ga age for granites in the northern Gawler Craton is temporally discrete from Hiltaba-aged magmatism and defines a second period of A-type magmatism in the Gawler Craton. However, any link between the overall tectonic setting of the ca. 1.45 Ga granites and Hiltaba-aged magmatism is unknown.

The drill holes containing ca. 1.45 Ga magmatic and metamorphic rocks encompass a region of approximately 1000 km^2 (Fig. 1, Table 1). It is difficult to determine the wider spatial footprint and structural architecture of ca. 1.45 Ga metamorphism due to the limited number of drill holes that intersect basement in this part of southern Australia. The remaining drill holes in the northern Gawler Craton intersect gneissic rocks that record the effects of the ca. 1.73–1.69 Ga Kimban Orogeny (Payne et al., 2008; Howard et al., 2011c), consistent with the inherited ca. 1.72 Ga zircon in the OBD 08 granite. Some regions of the northern Gawler Craton have also been overprinted by UHT metamorphism at ca. 1.59 Ga (Cutts et al., 2011). One implication of this polymetamorphic history is that the rocks of the northern Gawler Craton were likely to have lost significant volumes of melt, creating anhydrous, residual bulk compositions that were relatively resistant to reworking during subsequent metamorphic events (e.g. Rayner–Eastern Ghats terrane, Morrissey et al., 2016a; Wyoming Craton, Dragovic et al., 2016; Western Gneiss Region, Norway, Hacker et al., 2015). This may also mean that the record of ca. 1.45 Ga metamorphism is limited to rocks that had metamorphically reactive bulk compositions at or prior to ca. 1.45 Ga, such as zones of retrogression (e.g. Morrissey et al., 2016a), thereby limiting the apparent spatial extent of the event (albeit in a very sparsely sampled terrain). Alternatively, the ca. 1.45 Ga metamorphism in the northern Gawler Craton may be relatively spatially localised and predominantly driven by magmatism. However, apatite U–Pb data from throughout the Nawa Domain indicate a broader thermal event and suggests regional temperatures of ~550–350 °C at ca. 1.40–1.30 Ga (Hall et al., 2018), requiring either a regional heat source or volumetrically significant magmatism. Similarly, the presence of crustally-derived, interpreted A-type magmatism also indicates a larger region of elevated temperatures in the lower crust. The rocks in OBD 09 are foliated, suggesting that the event also involved some deformation. Therefore, although the high temperatures (~800 °C) recorded by the samples in drill hole OBD 09 are likely to be influenced by contact metamorphism, the overall thermal footprint of this event was regional. However, the lack of outcrop means it is difficult to determine the overall tectonic setting of ca. 1.45 Ga metamorphism. The A-type granites require a setting that allows high temperature partial melting of dehydrated, residual lower crust (Whalen et al., 1987; Frost et al., 2001). A-type granites are commonly attributed to extensional settings but can also form as a result of basaltic underplating during lithospheric delamination or mantle upwelling in convergent settings (Whalen et al., 1987; Smithies et al., 2011; Frost and Frost, 2013). Large northeast-trending shear zones in the northern and western Gawler Craton are interpreted to be part of a transpressional system and were active at ca. 1.45 Ga, but they have complex histories that likely involved multiple phases of reactivation in the Paleoproterozoic and Mesoproterozoic (Swain et al., 2005b; Thomas et al., 2008). The drill holes containing ca. 1.45 Ga rocks are located within the same geophysical domain as drill hole GOMA DH4, which records migmatisation at ca. 1.52 Ga of a ca. 2.53 Ga protolith. This domain sits between a series of north-dipping shear zones (Korsch et al., 2010). The new monazite data in this study supports the inference that at least some of the moderately dipping shear zones in the northern Gawler Craton reflect tectonism at ca. 1.52 Ga and/or ca. 1.45 Ga (e.g. Reid et al., 2014a). The multiple phases of reactivation along these shear zones and the absence of outcrop means that it is difficult to determine the character of deformation at ca. 1.45 Ga, or to distinguish between an overall extensional or transpressional tectonic setting. However, the interpretation of an extensional regime at ca. 1.45 Ga is supported by the development of rift basins in the SAC and NAC during this interval, discussed in more detail below.

5.2. Extent of ca. 1.50–1.45 Ga tectonism within the combined NAC/SAC

There remains some uncertainty as to the Proterozoic tectonic configuration of Australia and the timing of amalgamation of the cratons (e.g. Myers et al., 1996; Betts and Giles, 2006; Schmidt et al., 2006; Cawood and Korsch, 2008; Payne et al., 2009). The WAC and NAC are commonly proposed to have amalgamated by ca. 1.70 Ga, based on paleomagnetic data and the interpretation that the ca. 1.80–1.76 Ga Yapungku Orogeny in the Rudall Province involved high pressures and therefore records the collision of the WAC and NAC (Smithies and Bagas, 1997; Li, 2000; Bagas, 2004). However, the paleomagnetic data is based on poorly age-constrained poles in the Pilbara Craton in the WAC, and in addition, the paleomagnetic poles cannot provide any constraints on the relative palaeolongitudes of the two cratons. The timing of the high pressure event in the Rudall Province is also subject to debate, with new geochronology indicating that it occurred between 1.38 Ga and 1.27 Ga (Anderson et al., 2016). Cawood and Korsch (2008) and Payne et al. (2009) proposed a linked history for the NAC and SAC from the Archean to early Mesoproterozoic with subsequent rifting/rotation of the Mawson Continent/SAC at some time after ca. 1.59 Ga, commonly suggested to have occurred between 1.50 Ga and 1.35 Ga (Giles et al., 2004; Betts and Giles, 2006; Aitken et al., 2016). We therefore adopt a starting tectonic reconstruction that places the SAC adjacent to the NAC at ca. 1.45 Ga (Fig. 8). The WAC and rocks beneath the Eucla Basin have been excluded from the following discussion on the basis of uncertainty about their relationship to the NAC and SAC during this time period.

The ca. 1.45 Ga magmatism and metamorphism in the northern Gawler Craton was part of a widespread event at ca. 1.50–1.40 Ga in the NAC and SAC (Fig. 8). Lithospheric-scale shear zones in the Gawler Craton, including the Karari, Tallacootra, Coorabie and Kalinjala Shear Zones (Figs. 1 and 8), yield $^{40}Ar/^{39}Ar$ and monazite ages between 1.47 Ga and 1.45 Ga (Foster and Ehlers, 1998; Swain et al., 2005b; Fraser and Lyons, 2006; Thomas et al., 2008), suggesting that they were reactivated or underwent cooling at this time. Apatite U–Pb ages of ca. 1.40–1.30 Ga throughout the northern

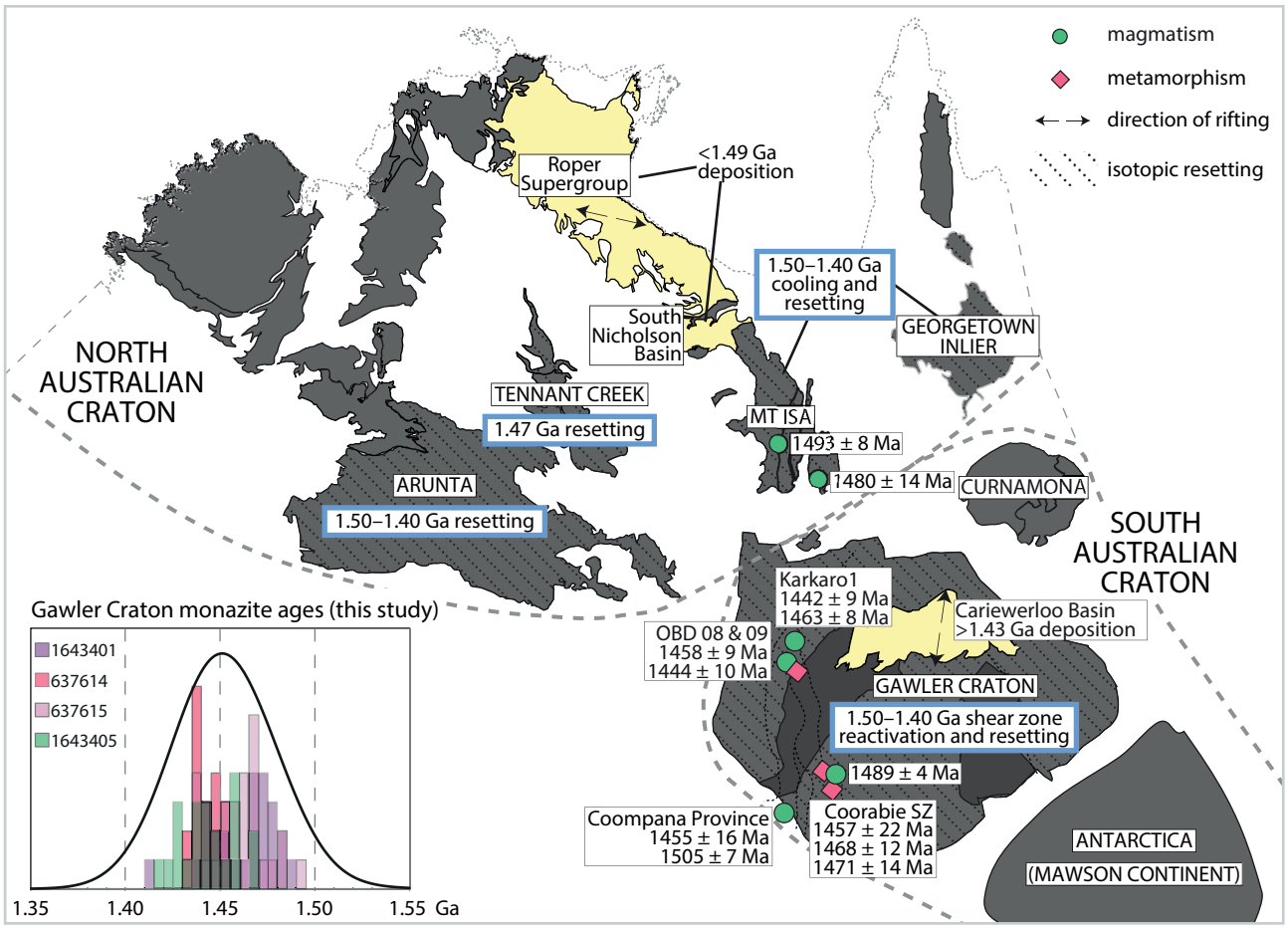

Figure 8. Compilation of 1.50–1.40 Ga record within the North Australian Craton (NAC) and South Australian Craton (SAC). In the southwest Gawler Craton, felsic magmatism, shear zone reactivation and metamorphism occurred between 1.50 Ga and 1.45 Ga. Within the NAC, felsic magmatism occurs in the Mount Isa Province at 1.50–1.48 Ga. Basin development is recorded in the Roper Group in the NAC and the Cariewerloo Basin in the SAC. Widespread isotopic resetting at 1.50–1.40 Ga occurred in rocks from the Georgetown Inlier, Mount Isa and Arunta Provinces and the Tanami and Tennant Creek regions. References for Fig. 8 are given in the text.

Gawler Craton are consistent with this interpretation (Hall et al., 2018). In the southwestern Gawler Craton (Fig. 8), U–Pb zircon dating of pegmatite intersected by mineral exploration drilling yields an age of 1489 ± 4 Ma (Fig. 8; Fanning et al., 2007). On the western edge of the Gawler Craton in the eastern Coompana Province (Fig. 8), granites sampled in petroleum well Mallabie-1 at a depth of around 1400 m give zircon U–Pb ages ranging between 1505 ± 7 Ma (Wade et al., 2007) and 1455 ± 16 Ma (Fanning et al., 2007). Within the NAC, the youngest phase of the Williams Batholith in the eastern Mount Isa region has a U–Pb age of 1493 ± 8 Ma (Page and Sun, 1998). This was approximately coeval with pegmatite intrusions at 1480 ± 14 Ma in the western Mount Isa region (Connors and Page, 1995). Modern day stream sediment from the eastern Mount Isa region contains a large proportion (~14%) of 1.50–1.40 Ga zircon grains (Condie et al., 2011), suggesting magmatism of this age may be more widespread than currently documented from outcrop. Further evidence for a thermal event in this part of Proterozoic Australia comes from widespread resetting of the Rb–Sr system (e.g. Black et al., 1979; Shaw and Black, 1991) and ^{40}Ar–^{39}Ar cooling ages of ca. 1.50–1.40 Ga in the NAC (Black et al., 1979; Spikings et al., 2002).

In addition to the record of shear zone reactivation, magmatism and isotopic resetting between 1.50 Ga and 1.40 Ga, this interval also involved the development of rift basins (Fig. 8). In the Gawler Craton, the Pandurra Formation, basal unit to the Cariewerloo Basin, is interpreted to have a minimum depositional age of ca. 1.49 Ga based on the oldest $^{40}Ar/^{39}Ar$ age for diagenetic illite (Beyer et al., 2018). A younger $^{40}Ar/^{39}Ar$ age of ca. 1.45 Ga is interpreted to reflect fluid flow (Beyer et al., 2018), and is similar to a ca. 1.42 Ga Rb–Sr whole rock age for Pandurra Formation siltstone (Fanning et al., 1983) and a ca. 1.44 Ga age for diagenetic apatite in Pandurra Formation equivalents in the Olympic Dam region (Cherry et al., 2017). The sedimentology of the Pandurra Formation facies suggests they were deposited in half grabens in fluvial and lacustrine paleo-environments as part of a continental rift system. Intracratonic rifting is proposed to have resulted from an extensional regime established as the Gawler Craton underwent dextral rotation (Beyer et al., 2018). In northern Australia, approximately coeval east–west directed rift basin development in the lower Roper Group occurred at ca. 1.49 Ga (Fig. 8; Jackson et al., 1999 and references therein). The Roper Group is interpreted to have formed in an intracratonic rift setting on the NAC (Betts and Giles, 2006), with the extensional setting nominated as related to the rifting of Australia and Laurentia (Yang et al., 2018). Conversely, the sequence stratigraphy of the middle Roper Group (which encapsulates the relevant period for this study) has been used to interpret deposition due to flexural accommodation in a foreland basin setting (Abbot and Sweet, 2000). The causative orogen for such a setting has not been identified, and although metamorphism and magmatism recorded in the northern Gawler Craton could be a candidate for the orogen required for a foreland ramp-style basin for the middle Roper Group, we do not consider this to be the over-riding tectonic setting of Australia. The character of magmatism and

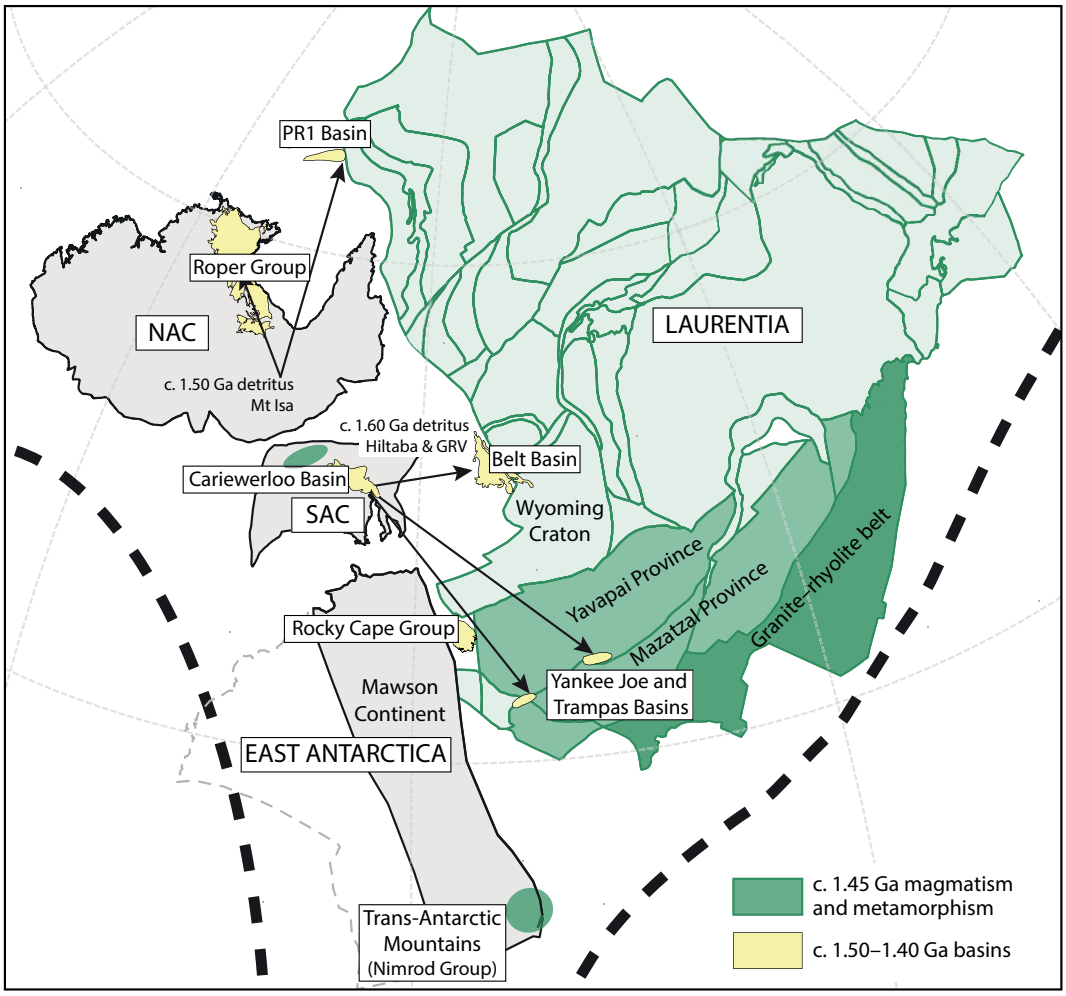

Figure 9. Proposed tectonic reconstruction for the North Australian Craton, Mawson Continent and Laurentia at ca. 1.45 Ga, depicted using G-Plates. Polygons adapted from Pehrsson et al. (2015) (Laurentia), Aitken et al. (2014) and Halpin et al. (2014) (Mawson Continent) and Geoscience Australia (www.ga.gov.au).

metamorphism in the northern Gawler Craton, and the widespread, relatively synchronous cooling/exhumation of the SAC and NAC suggests a broadly extensional setting is suitable for the SAC and NAC at ca. 1.45 Ga.

5.3. Extent of ca. 1.50–1.45 Ga tectonism in Laurentia

Laurentia is commonly proposed to be contiguous with the combined NAC/Mawson Continent in Nuna reconstructions (e.g. Zhao et al., 2002; Evans and Mitchell, 2011; Zhang et al., 2012; Pisarevsky et al., 2014; Pehrsson et al., 2015). The 1.50–1.40 Ga interval in Laurentia involved widespread granitic magmatism, high-temperature, low-pressure metamorphism, rift basin development and isotopic resetting.

Southern Laurentia contains an extensive belt of A-type granites and related anorthosites that were emplaced in two stages at 1.50–1.40 Ga and ca. 1.39–1.34 Ga (Fig. 9; e.g. Goodge and Vervoort, 2006; Bickford et al., 2015). The granite belt trends southwest to northeast from northwestern Mexico to Ontario (Anderson and Cullers, 1999; Goodge and Vervoort, 2006; Whitmeyer and Karlstrom, 2007; Jones et al., 2010a). The granites intrude Proterozoic crust with ages between 2.00 Ga and 1.60 Ga and are interpreted to be crustally derived (Goodge and Vervoort, 2006). The granites are variably deformed, which has led to debate as to the character of the ca. 1.40 Ga event (e.g. Nyman et al., 1994; Siddoway et al., 2000; Goodge and Vervoort, 2006). However, metasedimentary sequences in Arizona and New Mexico that were presumed to be Paleoproterozoic have protolith ages between ca. 1.49 Ga and 1.44 Ga (Jones et al., 2011; Doe et al., 2012; Daniel et al., 2013), suggesting they were deformed and metamorphosed during a significant regional Mesoproterozoic event (Picuris Orogeny; Daniel et al., 2013). The Picuris Orogeny involved reactivation of northeast-striking shear zones, contractional to strike-slip deformation in contact aureoles of ca. 1.45 Ga plutons and fold-and-thrust-style deformation of metasedimentary rocks (Nyman et al., 1994; Daniel et al., 2013). Widespread, high thermal gradient (andalusite–sillimanite) metamorphism occurs throughout southern Laurentia at 1.47–1.37 Ga (Nyman et al., 1994; Nyman and Karlstrom, 1997; Selverstone et al., 2000; Siddoway et al., 2000; Daniel and Pyle, 2006; Jones et al., 2010b). The contractional deformation and regional metamorphism are used to argue that the Picurus Orogeny occurred in an active compressional or transpressional setting (Nyman et al., 1994; Karlstrom et al., 2001; Daniel et al., 2013), consistent with the suggestion that the southern margin of Laurentia was a long-lived convergent margin between ca. 1.80 Ga and 1.10 Ga (Karlstrom et al., 2001; Whitmeyer and Karlstrom, 2007).

The interval between ca. 1.50 Ga and 1.40 Ga also involved the development of extensional domains and widespread deposition of sedimentary successions throughout Laurentia, including the thick Belt–Purcell Supergroup (ca. 1.47–1.40 Ma; Evans et al., 2000), Hess Canyon Group in Arizona (1.49–1.44 Ga; Doe et al., 2012) and Trampas basin in New Mexico (1.49–1.45 Ga; Daniel et al., 2013).

The sedimentary successions in each of these basins can be broadly divided into pre-1.45 Ga and post-1.45 Ga successions based on different detrital zircon spectra and an inferred shift in provenance (Jones et al., 2015). The basin successions deposited prior to 1.45 Ga contain abundant detrital zircon with ages of 1.61–1.49 Ga, which correspond to the timing of magmatic events in the Gawler Craton, northern Australia and east Antarctica (Ross et al., 1992; Ross and Villeneuve, 2003; Doe et al., 2012, 2013; Daniel et al., 2013). In the Yukon region of northern Laurentia, the lower PR1 basin is also inferred to be broadly coeval and has a unimodal detrital zircon population at ca. 1.50 Ga, interpreted to be derived from the youngest phases of 1.55–1.49 Ga granitic magmatism in the eastern Mount Isa region (Medig et al., 2014). Post 1.45 Ga, Laurentian sedimentary successions do not contain 1.60–1.50 Ga detrital zircon and are instead dominated by 1.86–1.64 Ga ages that are interpreted to be derived from a southern Laurentian or east Antarctic source (e.g. Ross and Villeneuve, 2003; Stewart et al., 2010). Sedimentary rocks in Tasmania (Rocky Cape Group) deposited between 1.45 Ga and 1.33 Ga also have Laurentian or east Antarctica provenance and are proposed to be equivalents of the upper Belt–Purcell stratigraphy (Halpin et al., 2014; Mulder et al., 2015). The shift from Australian-derived to Laurentian/east Antarctic-derived sources at ca. 1.45 Ga has been interpreted to reflect either final separation of Australia and western Laurentia (e.g. Betts and Giles, 2006) or changing basin architecture as a result of contractional orogenesis and regional uplift in southern Laurentia during the Picuris Orogeny at ca. 1.45 Ga (Jones et al., 2015).

The widespread magmatism, high thermal gradient metamorphism and deformation in Laurentia is coeval with, and stylistically similar to, the ca. 1.50–1.40 Ga event throughout eastern Australia. The similarities in timing, style and scale of this event in both continents strengthens support for a connection between Australia and Laurentia in Nuna reconstructions and raises the possibility that the two events can be directly linked. However, there are no reliable paleomagnetic constraints for Australia in the interval 1.50–1.22 Ga (Pisarevsky et al., 2014), meaning that the positioning of Australia along the western margin of Laurentia is more contentious, as is the timing of separation. These uncertainties mean the newly recognised ca. 1.45 Ga metamorphism from the northern Gawler Craton and widespread 1.50–1.40 Ga tectonism throughout the NAC and SAC can be interpreted in several ways in the context of tectonic reconstructions.

5.4. Interpretation 1: correlations to the Laurentian ca. 1.50–1.40 Ga event

The most widely used configuration in Nuna reconstructions is a proto-SWEAT connection, which places southern Laurentia adjacent to East Antarctica and Australia adjacent to Canada (e.g. Payne et al., 2009; Evans and Mitchell, 2011; Zhang et al., 2012; Pisarevsky et al., 2014). In this reconstruction, the 1.47–1.37 Ga granite belt in Laurentia is correlated with the Nimrod Glacier region of the Trans-Antarctic Mountains in East Antarctica. The Trans-Antarctic Mountains contain clasts of 1.50–1.41 Ga granite that isotopically and geochemically overlap with those from southern Laurentia (Goodge et al., 2008, 2017). Neoproterozoic to Cambrian sedimentary rocks in the Trans-Antarctic Mountains also contain significant proportions (~22%) of ca. 1.40 Ga zircon with Hf signatures that correspond to the ca. 1.40 Ga Laurentian granites, which was interpreted as further evidence for an extension of the Laurentian granite belt beneath the ice (Goodge et al., 2008). A less commonly used reconstruction correlates the Laurentian granites with ca. 1.43 Ga gneissic granitoids of the Baoban Complex in Hainan Island, southwest Cathaysia (Li et al., 2008a). These have similar age, chemistry and Nd and Pb isotopes to the Laurentian A-type granites (Li et al., 2002, 2008a). However, this configuration was originally proposed for Rodinia reconstructions (Li et al., 2008b) and is not universally adopted in Nuna reconstructions.

The recognition of 1.45 Ga A-type magmatism and high thermal gradient metamorphism in the northern Gawler Craton could provide another candidate for the continuation of the Laurentian granite–rhyolite belt. Metamorphic grade in Laurentia is variable, but is generally high thermal gradient (andalusite–sillimanite) and associated with magmatism (Goodge and Siddoway, 1997; Daniel and Pyle, 2006). The high thermal gradient metamorphism in both continents was accompanied by reactivation of older shear zones, basin development and widespread isotopic resetting, further supporting the interpretation that the event was stylistically similar. On face value, Australia contains more evidence for a widespread ca. 1.50–1.40 Ga event than Antarctica, where the record of the ca. 1.45 Ga event is confined to the Trans-Antarctic Mountains. However, as much of Antarctica and parts of Australia are poorly outcropping, it is difficult to determine the apparent spatial extent of this event.

Assuming that the ca. 1.50–1.40 Ga event in Australia and Laurentia reflects a single contiguous zone of active tectonism, albeit with along-strike variation between transpressional and extensional or transtensional stress regimes, we propose a reconstruction at ca. 1.45 Ga that places the Gawler Craton further south than the traditional proto-SWEAT reconstruction (Fig. 9), visualised using G-Plates software (www.gplates.org). The continental fragments used in this reconstruction are modern day equivalents, which necessarily introduces some uncertainty as the amount of post-1.45 Ga extension, compression and crustal growth, particularly within the ice-covered Mawson Continent, is unknown. Our model allows the Gawler Craton to be placed closer to the belt of ca. 1.45 Ga magmatism and metamorphism that characterises southern Laurentia, rather than adjacent to Canada where there is no significant record of the ca. 1.45 Ga event (Whitmeyer and Karlstrom, 2007). In this scenario, the northern Gawler Craton is placed in an intracontinental extensional setting, inboard of the compressional/transpressional setting recorded by the Picuris Orogeny in southern Laurentia (Nyman et al., 1994; Karlstrom et al., 2001; Daniel et al., 2013). This reconstruction also places the most significant source of ca. 1.6–1.58 Ga zircons (the Hiltaba Suite and Gawler Range Volcanics) in proximity to the Belt Basin and smaller basins in southern Laurentia, as is proposed by some sedimentary provenance studies (e.g. Stewart et al., 2010; Doe et al., 2012; Jones et al., 2015; Verbaas et al., 2018). Assuming the Antarctic part of the Mawson Continent was a similar length scale to what is recorded today, our model also allows correlation between the southern margin of Laurentia and the Trans-Antarctic Mountains, consistent with the recognition of tectonism and crustal growth at ca. 1.45 Ga and at ca. 1.3–1.00 Ga in southern Laurentia (Whitmeyer and Karlstrom, 2007) and in glacial clasts in the Trans-Antarctic Mountains (Goodge et al., 2017). It also consistent with the sedimentary provenance studies that argue for a direct connection between Mount Isa and northern Laurentia (Medig et al., 2014), as northern Australia is proximal to northern Laurentia. A configuration that places Australia even further south and directly correlates the northern Gawler Craton with the southern margin of Laurentia (e.g. AUSWUS; Karlstrom et al., 2001) would mean the Mawson Continent forms a large peninsula with no obvious east-ward extension, which is not consistent with the geology observed in the Trans-Antarctic Mountains.

5.5. Interpretation 2: correlation without connection between Australia and Laurentia

All the scenarios that extend the 1.47–1.37 Ga Laurentian granite–rhyolite belt into conjugate continents require Nuna breakup to have occurred after 1.45–1.43 Ga, depending on the

precise timing of magmatism and metamorphism in the correlated continent (e.g. this study; Goodge et al., 2008; Li et al., 2008a). However, the timing of separation of Australia and Laurentia is unconstrained (e.g. Pisarevsky et al., 2014), raising the possibility that Laurentia and Australia had separated prior to ca. 1.45 Ga. In this scenario, the magmatism and metamorphism in the northern Gawler Craton cannot be a direct correlative of the Laurentian granite-rhyolite belt.

The ca. 1.50–1.45 Ga tectonism recorded in the northern Gawler Craton is coeval with the change in sedimentary sources within the ca. 1.49–1.40 Ga basins in southern Laurentia (e.g. Jones et al., 2015). This has been proposed to reflect the removal of the Australia–Mawson Continent from western Laurentia (Betts and Giles, 2006) and/or changing basin architecture as a result of regional uplift in southern Laurentia during the Picuris Orogeny at ca. 1.45 Ga (Daniel et al., 2013; Jones et al., 2015). Although common Rodinia reconstructions place Australia in proximity to western Laurentia, similar to Nuna reconstructions (Li et al., 2008b; Merdith et al., 2017), many require some translation of Australia along the western margin of Rodinia. Alternative reconstructions suggest Australia and Laurentia were widely separated or in radically different configurations in Rodinia (Evans, 2009; Pisarevsky et al., 2014). The ca. 1.50–1.40 Ga basins of Australia and Laurentia occur along the inferred rifted margin (Fig. 9), providing support for the breakup of the two continents.

Several models have been proposed for the breakup of Australia and Laurentia. One (assuming a proto-SWEAT configuration), suggests that the separation of Australia and Laurentia began with rifting between the Mawson Continent and southern Laurentia, the timing of which is unconstrained (Pisarevsky et al., 2014). Rifting then propagated northward, before final breakup between the NAC and Laurentia at ca. 1.38 Ga (Pisarevsky et al., 2014). An alternative model suggests that rifting propagated southward at ca. 1.45 Ga, removing the NAC and SAC but leaving a connection between Laurentia and east Antarctica during the deposition of the upper Belt supergroup and coeval basins in southern Laurentia and Tasmania (Stewart et al., 2010; Jones et al., 2015; Mulder et al., 2015). In either scenario, the ca. 1.45 Ga magmatism and high thermal gradient metamorphism may reflect the response of both the northern Gawler Craton and Laurentia to the onset of extension and rifting, but without requiring a direct correlation between the two metamorphic belts. This event may have also involved reorganisation of the Australian cratons and possible rotation of the NAC relative to the SAC/Mawson Continent (Giles et al., 2004; Betts and Giles, 2006). The ca. 1.45 Ga reactivation of shear zones in the northern Gawler may reflect transmission of these boundary stresses into the interior of the continent.

6. Conclusions

Monazite U–Pb geochronology from three drill holes in the northern Gawler Craton reveals the presence of a previously unrecognised event at ca. 1.45 Ga. Calculated metamorphic phase diagrams suggest that this event reached pressures of 3.2–5.4 kbar and temperatures of 775–815 °C. Undeformed and unmetamorphosed ca. 1.45 Ga granitic rocks intersected in two drill holes have steep LREE-enriched patterns and high Ga/Al values suggesting they are A-type granites. The ca. 1.45 Ga magmatism and metamorphism in the northern Gawler Craton was part of a widespread event at ca. 1.50–1.40 Ga in the NAC and SAC that involved shear zone reactivation, magmatism and rift basin development and is considered to indicate a dominantly extensional event in proto-Australia at that time. This event is stylistically similar to some aspects of ca. 1.45 Ga A-type magmatism, sedimentation and high thermal gradient metamorphism throughout southern Laurentia. This may indicate a closer connection between the Gawler Craton and southern Laurentia, in contrast to 'proto-SWEAT' reconstructions that place Australia adjacent to northern Laurentia. Further research is required to determine if this timeframe can be unequivocally linked to the breakup of Australia and Laurentia, but the recognition of ca. 1.45 Ga magmatism and metamorphism in the northern Gawler Craton lends support to models proposing a reorganisation of the proto-Australian crustal elements at this time.

Acknowledgements

The staff at Adelaide Microscopy are thanked for technical assistance and the staff at the South Australian Drill Core Reference Library are thanked for assistance with sampling. Andrew Merdith is thanked for assistance with G-Plates. Karl Karlstrom and an anonymous reviewer are thanked for constructive review comments that improved the manuscript. This project was supported by ARC Linkage Project LP160100578 (MH and JP) and ARC Discovery Project DP160104637 (MH).

Appendix A. Supplementary data

Supplementary data related to this article can be found at https://doi.org/10.1016/j.gsf.2018.07.006.

References

Abbot, S.T., Sweet, I.P., 2000. Tectonic control on third-order sequences in a siliciclastic ramp-style basin: an example from the Roper Superbasin (Mesoproterozoic), Northern Australia. Australian Journal of Earth Sciences 47, 637–657.
Aitken, A.R.A., Betts, P.G., Young, D.A., Blankenship, D.D., Roberts, J.L., Siegert, M.J., 2016. The Australo-Antarctic Columbia to Gondwana transition. Gondwana Research 29, 136–152.
Aitken, A.R.A., Young, D.A., Ferraccioli, F., Betts, P.G., Greenbaum, J.S., Richter, T.G., Roberts, J.L., Blankenship, D.D., Siegert, M.J., 2014. The subglacial geology of Wilkes Land, east Antarctica. Geophysical Research Letters 41, 2390–2400.
Aleinikoff, J.N., Schenck, W.S., Plank, M.O., Srogi, L.A., Fanning, C.M., Kamo, S.L., Bosbyshell, H., 2006. Deciphering igneous and metamorphic events in high-grade rocks of the Wilmington complex, Delaware: morphology, cathodoluminescence and backscattered electron zoning, and SHRIMP U-Pb geochronology of zircon and monazite. Bulletin of the Geological Society of America 118, 39–64.
Anderson, J.L., Bender, E.E., 1989. Nature and origin of Proterozoic A-type granitic magmatism in the southwestern United States of America. Lithos 23, 19–52.
Anderson, J.L., Cullers, R.L., 1999. Paleo- and Mesoproterozoic granite plutonism of Colorado and Wyoming. Rocky Mountain Geology 34, 149–164.
Anderson, J.R., Kelsey, D.E., Hand, M., Collins, W.J., 2013. Conductively driven, high-thermal gradient metamorphism in the Anmatjira Range, Arunta region, central Australia. Journal of Metamorphic Geology 31, 1003–1026.
Anderson, J.R., Kelsey, D.E., Hand, M., Collins, W.J., 2016. Mesoproterozoic Metamorphism in the Rudall Province: Revising the Timeline of the Yapungku Orogeny and Implications for Cratonic Australia Assembly, Australian Earth Sciences Convention 2016: Uncover the Earth's Past to Discover Our Future. AESC Abstracts, Adelaide, p. 228.
Armit, R., Betts, P.G., Schaefer, B.F., Yi, K., Kim, Y., Dutch, R.A., Reid, A., Jagodzinski, L., Giles, D., Ailleres, L., 2017. Late Palaeoproterozoic evolution of the buried northern Gawler Craton. Precambrian Research 291, 178–201.
Bagas, L., 2004. Proterozoic evolution and tectonic setting of the northwest Paterson Orogen, Western Australia. Precambrian Research 128, 475–496.
Betts, P.G., Armit, R.J., Stewart, J., Aitken, A.R.A., Ailleres, L., Donchak, P., Hutton, L., Withnall, I., Giles, D., 2016. Australia and Nuna. In: Li, Z.X., Evans, D.A.D., Murphy, J.B. (Eds.), Supercontinent Cycles through Earth History. Geological Society, London, pp. 47–81. Special Publications.
Betts, P.G., Giles, D., 2006. The 1800-1100 Ma tectonic evolution of Australia. Precambrian Research 144, 92–125.
Betts, P.G., Giles, D., Schaefer, B.F., 2008. Comparing 1800-1600 Ma accretionary and basin processes in Australia and Laurentia: possible geographic connections in Columbia. Precambrian Research 166, 81–92.
Beyer, S.R., Kyser, K., Polito, P.A., Fraser, G.L., 2018. Mesoproterozoic rift sedimentation, fluid events and uranium prospectivity in the Cariewerloo Basin, Gawler Craton, South Australia. Australian Journal of Earth Sciences 65, 409–426.
Bickford, M.E., Van Schmus, W.R., Karlstrom, K.E., Mueller, P.A., Kamenov, G.D., 2015. Mesoproterozoic-trans-Laurentian magmatism: a synthesis of continent-wide age distributions, new SIMS U–Pb ages, zircon saturation temperatures, and Hf and Nd isotopic compositions. Precambrian Research 265, 286–312.

Black, L.P., Bell, T.H., Rubenach, M.J., Withnall, I.W., 1979. Geochronology of discrete structural-metamorphic events in a multiply deformed precambrian terrain. Tectonophysics 54, 103–137.
Boger, S.D., Hansen, D., 2004. Metamorphic evolution of the Georgetown Inlier, northeast Queensland, Australia; evidence for an accreted Palaeoproterozoic terrane? Journal of Metamorphic Geology 22, 511–527.
Boyd, F., Mertzman, S., 1987. Composition and structure of the Kaapvaal lithosphere, southern Africa. In: Mysen, B.O. (Ed.), Magmatic Processes: Physicochemical Principles. Geochemical Society Special Publication, pp. 13–24.
Boynton, W.V., 1984. Cosmochemistry of the rare earth elements: meteorite studies. Developments in Geochemistry 2, 63–114.
Cawood, P.A., Hawkesworth, C.J., 2015. Temporal relations between mineral deposits and global tectonic cycles. In: Jenkin, G.R.T., Lusty, P.A.J., McDonald, I., Smith, M.P., Boyce, A.J., Wilkinson, J.J. (Eds.), Ore Deposits in an Evolving Earth. Geological Society, London, Special Publications, pp. 9–21.
Cawood, P.A., Korsch, R.J., 2008. Assembling Australia: Proterozoic building of a continent. Precambrian Research 166, 1–35.
Cherry, A.R., McPhie, J., Kamenetsky, V.S., Ehrig, K., Keeling, J.L., Kamenetsky, M.B., Meffre, S., Apukhtina, O.B., 2017. Linking Olympic Dam and the Cariewerloo Basin: was a sedimentary basin involved in formation of the world's largest uranium deposit? Precambrian Research 300, 168–180.
Condie, K.C., Aster, R.C., 2010. Episodic zircon age spectra of orogenic granitoids: the supercontinent connection and continental growth. Precambrian Research 180, 227–236.
Condie, K.C., Bickford, M.E., Aster, R.C., Belousova, E., Scholl, D.W., 2011. Episodic zircon ages, Hf isotopic composition, and the preservation rate of continental crust. GSA Bulletin 123, 951–957.
Connors, K.A., Page, R.W., 1995. Relationships between magmatism, metamorphism and deformation in the western Mount Isa Inlier, Australia. Precambrian Research 71, 131–153.
Conor, C.H.H., Preiss, W.V., 2008. Understanding the 1720–1640 Ma Palaeoproterozoic Willyama supergroup, Curnamona province, southeastern Australia: implications for tectonics, basin evolution and ore genesis. Precambrian Research 166, 297–317.
Cutts, K., Hand, M., Kelsey, D.E., 2011. Evidence for early Mesoproterozoic (ca. 1590Ma) ultrahigh-temperature metamorphism in southern Australia. Lithos 124, 1–16.
Daly, S.J., Fanning, C.M., Fairclough, M.C., 1998. Tectonic evolution and exploration potential of the Gawler craton, south Australia. AGSO Journal of Australia Geology and Geophysics 17, 145–168.
Daniel, C.G., Pfeifer, L.S., Jones, J.V., McFarlane, C.M., 2013. Detrital zircon evidence for non-Laurentian provenance, Mesoproterozoic (ca. 1490–1450 Ma) deposition and orogenesis in a reconstructed orogenic belt, northern New Mexico, USA: defining the Picuris orogeny. Geological Society of America Bulletin 125, 1423–1441.
Daniel, C.G., Pyle, J.M., 2006. Monazite–xenotime Thermochronometry and Al2SiO5 reaction textures in the Picuris range, northern New Mexico, USA: new evidence for a 1450–1400 Ma orogenic event. Journal of Petrology 47, 97–118.
Diener, J.F.A., White, R.W., Powell, R., 2008. Granulite facies metamorphism and subsolidus fluid-absent reworking, Strangways Range, Arunta Block, central Australia. Journal of Metamorphic Geology 26, 603–622.
Doe, M.F., Jones Iii, J.V., Karlstrom, K.E., Dixon, B., Gehrels, G., Pecha, M., 2013. Using detrital zircon ages and Hf isotopes to identify 1.48–1.45 Ga sedimentary basins and fingerprint sources of exotic 1.6–1.5 Ga grains in southwestern Laurentia. Precambrian Research 231, 409–421.
Doe, M.F., Jones, J.V., Karlstrom, K.E., Thrane, K., Frei, D., Gehrels, G., Pecha, M., 2012. Basin formation near the end of the 1.60–1.45 Ga tectonic gap in southern Laurentia: Mesoproterozoic Hess Canyon Group of Arizona and implications for ca. 1.5 Ga supercontinent configurations. Lithosphere 4, 77–88.
Dragovic, B., Guevara, V.E., Caddick, M.J., Baxter, E.F., Kylander-Clark, A.R.C., 2016. A pulse of cryptic granulite-facies metamorphism in the Archean Wyoming Craton revealed by Sm–Nd garnet and U–Pb monazite geochronology. Precambrian Research 283, 24–49.
Dutch, R., Hand, M., Kinny, P.D., 2008. High-grade Paleoproterozoic reworking in the southeastern Gawler craton, south Australia. Australian Journal of Earth Sciences 55, 1063–1081.
Dutch, R.A., Hand, M., Kelsey, D.E., 2010. Unravelling the tectonothermal evolution of reworked Archean granulite facies metapelites using in situ geochronology: an example from the Gawler Craton, Australia. Journal of Metamorphic Geology 28, 293–316.
Evans, D.A.D., 2009. The palaeomagnetically viable, long-lived and all-inclusive Rodinia supercontient reconstruction. In: Murphy, J.B., Keppie, J.D., Hynes, A.J. (Eds.), Ancient Orogens and Modern Analogues. Geological Society of London Special Publications, pp. 371–404.
Evans, D.A.D., Mitchell, R.N., 2011. Assembly and breakup of the core of Paleoproterozoic–Mesoproterozoic supercontinent Nuna. Geology 39, 443–446.
Evans, K.V., Aleinikoff, J.N., Obradovich, J.D., Fanning, C.M., 2000. SHRIMP U-Pb geochronology of volcanic rocks, Belt Supergroup, western Montana: evidence for rapid deposition of sedimentary strata. Canadian Journal of Earth Sciences 37, 1287–1300.
Fanning, C.M., Flint, R.B., Parker, A.J., Ludwig, K.R., Blissett, A.H., 1988. Refined Proterozoic evolution of the Gawler craton, south Australia, through U-Pb zircon geochronology. Precambrian Research 40–41, 363–386.
Fanning, C.M., Flint, R.B., Preiss, W.V., 1983. Geochronology of the Pandurra Formation. South Australia. Geological Survey Quarterly Geological Notes 88, 11–16.
Fanning, C.M., Reid, A.J., Teale, G.S., 2007. A geochronological framework for the Gawler craton, south Australia, south Australia. Geological Survey Bulletin 55.
Forbes, C.J., Giles, D., Hand, M., Betts, P.G., Suzuki, K., Chalmers, N., Dutch, R., 2011. Using P–T paths to interpret the tectonothermal setting of prograde metamorphism: an example from the northeastern Gawler Craton, South Australia. Precambrian Research 185, 65–85.
Forbes, C.J., Giles, D., Jourdan, F., Sato, K., Omori, S., Bunch, M., 2012. Cooling and exhumation history of the northeastern Gawler craton, south Australia. Precambrian Research 200–203, 209–238.
Foster, D.A., Ehlers, K., 1998. 40Ar-39Ar thermochronology of the southern Gawler craton, Australia: implications for Mesoproterozoic and Neoproterozoic tectonics of east Gondwana and Rodinia. Journal of Geophysical Research 103, 10177–10193.
Fraser, G., McAvaney, S., Neumann, N., Szpunar, M., Reid, A., 2010. Discovery of early Mesoarchean crust in the eastern Gawler craton, south Australia. Precambrian Research 179, 1–21.
Fraser, G., Reid, A., Stern, R., 2012. Timing of deformation and exhumation across the Karari shear zone, north-western Gawler craton, south Australia. Australian Journal of Earth Sciences 59, 547–570.
Fraser, G.L., Lyons, P., 2006. Timing of Mesoproterozoic tectonic activity in the northwestern Gawler Craton constrained by 40Ar/39Ar geochronology. Precambrian Research 151, 160–184.
Frost, B.R., Barnes, C.G., Collins, W.J., Arculus, R.J., Ellis, D.J., Frost, C.D., 2001. A geochemical Classification for granitic rocks. Journal of Petrology 42, 2033–2048.
Frost, C.D., Frost, B.R., 2013. Proterozoic ferroan feldspathic magmatism. Precambrian Research 228, 151–163.
Giles, D., Betts, P.G., Lister, G.S., 2004. 1.8-1.5-Ga links between the north and south Australian cratons and the early-middle Proterozoic configuration of Australia. Tectonophysics 380, 27–41.
Goodge, J., Siddoway, C., 1997. Mineral reactions and Petrogenetic Implications of Fe-mn-andalusite, Northern Wet Mountains, Colorado: Geological Society of America Abstracts with Programs, p. 11.
Goodge, J.W., Fanning, C.M., Fisher, C.M., Vervoort, J.D., 2017. Proterozoic crustal evolution of central East Antarctica: age and isotopic evidence from glacial igneous clasts, and links with Australia and Laurentia. Precambrian Research 299, 151–176.
Goodge, J.W., Vervoort, J.D., 2006. Origin of Mesoproterozoic A-type granites in Laurentia: Hf isotope evidence. Earth and Planetary Science Letters 243, 711–731.
Goodge, J.W., Vervoort, J.D., Fanning, C.M., Brecke, D.M., Farmer, G.L., Williams, I.S., Myrow, P.M., DePaolo, D.J., 2008. A positive test of East Antarctica-Laurentia juxtaposition within the Rodinia supercontinent. Science 321, 235–240.
Groves, D.I., Condie, K.C., Goldfarb, R.J., Hronsky, J.M.A., Vielreicher, R.M., 2005. 100th Anniversary special Paper: secular changes in global tectonic processes and their influence on the temporal distribution of Gold-bearing mineral deposits. Economic Geology 100, 203–224.
Hacker, B.R., Kylander-Clark, A.R.C., Holder, R., Andersen, T.B., Peterman, E.M., Walsh, E.O., Munnikhuis, J.K., 2015. Monazite response to ultrahigh-pressure subduction from U–Pb dating by laser ablation split stream. Chemical Geology 409, 28–41.
Hall, J.W., Glorie, S., Reid, A.J., Boone, S.C., Collins, A.S., Gleadow, A., 2018. An apatite U–Pb thermal history map for the northern Gawler Craton, South Australia. Geoscience Frontiers 9 (5), 1293–1308.
Halpin, J.A., Jensen, T., McGoldrick, P., Meffre, S., Berry, R.F., Everard, J.L., Calver, C.R., Thompson, J., Goemann, K., Whittaker, J.M., 2014. Authigenic monazite and detrital zircon dating from the Proterozoic Rocky Cape Group, Tasmania: links to the belt-Purcell supergroup, north America. Precambrian Research 250, 50–67.
Halpin, J.A., Reid, A.J., 2016. Earliest Paleoproterozoic high-grade metamorphism and orogenesis in the Gawler Craton, South Australia: the southern cousin in the Rae family? Precambrian Research 276, 123–144.
Hand, M., Reid, A.J., Jagodzinski, E., 2007. Tectonic framework and evolution of the Gawler craton, southern Australia. Economic Geology 102, 1377–1395.
Holland, T.J.B., Powell, R., 2011. An improved and extended internally consistent thermodynamic dataset for phases of petrological interest, involving a new equation of state for solids. Journal of Metamorphic Geology 29, 333–383.
Howard, K.E., Hand, M., Barovich, K., Belousova, E., 2011a. Provenance of late Paleoproterozoic cover sequences in the central Gawler Craton: exploring stratigraphic correlations in eastern Proterozoic Australia using detrital zircon ages, Hf and Nd isotopic data. Australian Journal of Earth Sciences 58, 475–500.
Howard, K.E., Hand, M., Barovich, K.M., Payne, J.L., Belousova, E.A., 2011b. U–Pb, Lu–Hf and Sm–Nd isotopic constraints on provenance and depositional timing of metasedimentary rocks in the western Gawler Craton: implications for Proterozoic reconstruction models. Precambrian Research 184, 43–62.
Howard, K.E., Hand, M., Barovich, K.M., Payne, J.L., Cutts, K.A., Belousova, E.A., 2011c. U–Pb zircon, zircon Hf and whole-rock Sm–Nd isotopic constraints on the evolution of Paleoproterozoic rocks in the northern Gawler Craton. Australian Journal of Earth Sciences 58, 615–638.
Jackson, M.J., Sweet, I.P., Page, R.W., Bradshaw, B.E., 1999. The South Nicholson and roper groups: evidence for the early mesoproterozoic roper superbasin. In: Bradshaw, B.E., Scott, D.L. (Eds.), Integrated Basin Analysis of the Isa Superbasin using Seismic, Well-log and Geopotential Data: An Evaluation of the Economic Potential of the Northern Lawn Hill Platform Australian Geological Survey Organisation. Record 1999/19 36–45.
Jackson, S.E., Pearson, N.J., Griffin, W.L., Belousova, E.A., 2004. The application of laser ablation-inductively coupled plasma-mass spectrometry to in situ U-Pb zircon geochronology. Chemical Geology 211, 47–69.

Jagodzinski, E.A., Reid, A.J., Chalmers, N., Swain, G., Frew, R.A., Foudoulis, C., 2007. Compilation of SHRIMP U-Pb Geochronological Data for the Gawler Craton, South Australia. South Australian Department of Primary Industries and Resources. Report Book 2007/21.
Johnson, T.E., White, R.W., 2011. Phase equilibrium constraints on conditions of granulite-facies metamorphism at Scourie, NW Scotland. Journal of the Geological Society 168, 147–158.
Jones, J.V., Daniel, C.G., Doe, M.F., 2015. Tectonic and sedimentary linkages between the Belt-Purcell basin and southwestern Laurentia during the Mesoproterozoic, ca. 1.60–1.40 Ga. Lithosphere 7, 465–472.
Jones, J.V., Daniel, C.G., Frei, D., Thrane, K., 2011. Revised regional correlations and tectonic implications of Paleoproterozoic and Mesoproterozoic metasedimentary rocks in northern New Mexico, USA: new findings from detrital zircon studies of the Hondo Group, Vadito Group, and Marqueñas Formation. Geosphere 7, 974–991.
Jones, J.V., Rogers, S.A., Connelly, J.N., 2010a. U-Pb geochronology of Proterozoic granites in the Sawatch Range, central Colorado. U.S.A. Rocky Mountain Geology 45, 1–22.
Jones, J.V., Siddoway, C.S., Connelly, J.N., 2010b. Characteristics and implications of ca. 1.4 Ga deformation across a Proterozoic mid-crustal section, Wet Mountains, Colorado, USA. Lithosphere 2, 119–135.
Karlstrom, K.E., Åhäll, K.-I., Harlan, S.S., Williams, M.L., McLelland, J., Geissman, J.W., 2001. Long-lived (1.8–1.0 Ga) convergent orogen in southern Laurentia, its extensions to Australia and Baltica, and implications for refining Rodinia. Precambrian Research 111, 5–30.
Kelsey, D.E., Hand, M., 2015. On ultrahigh temperature crustal metamorphism: phase equilibria, trace element thermometry, bulk composition, heat sources, timescales and tectonic settings. Geoscience Frontiers 6, 311–356.
Kirkland, C.L., Johnson, S.P., Smithies, R.H., Hollis, J.A., Wingate, M.T.D., Tyler, I.M., Hickman, A.H., Cliff, J.B., Tessalina, S., Belousova, E.A., Murphy, R.C., 2013a. Not-so-suspect terrane: constraints on the crustal evolution of the Rudall Province. Precambrian Research 235, 131–149.
Kirkland, C.L., Smithies, R.H., Spaggiari, C.V., 2015. Foreign contemporaries – unravelling disparate isotopic signatures from Mesoproterozoic central and western Australia. Precambrian Research 265, 218–231.
Kirkland, C.L., Smithies, R.H., Spaggiari, C.V., Wingate, M.T.D., Quentin de Gromard, R., Clark, C., Gardiner, N.J., Belousova, E.A., 2017. Proterozoic crustal evolution of the Eucla basement, Australia: implications for destruction of oceanic crust during emergence of Nuna. Lithos 278–281, 427–444.
Kirkland, C.L., Smithies, R.H., Woodhouse, A.J., Howard, H.M., Wingate, M.T.D., Belousova, E.A., Cliff, J.B., Murphy, R.C., Spaggiari, C.V., 2013b. Constraints and deception in the isotopic record; the crustal evolution of the west Musgrave Province, central Australia. Gondwana Research 23, 759–781.
Kirkland, C.L., Spaggiari, C.V., Pawley, M.J., Wingate, M.T.D., Smithies, R.H., Howard, H.M., Tyler, I.M., Belousova, E.A., Poujol, M., 2011. On the edge: U–Pb, Lu–Hf, and Sm–Nd data suggests reworking of the Yilgarn craton margin during formation of the Albany-Fraser Orogen. Precambrian Research 187, 223–247.
Korsch, R.J., Blewett, R.S., Giles, D., Reid, A., Neumann, N., Fraser, G.L., Holzschuh, J., Costelloe, R.D., Roy, I.G., Kennett, B.L.N., Cowley, W.M., Baines, G., Carr, L.K., Duan, J., Milligan, P.R., Armit, R., Betts, P.G., Preiss, W.V., Bendall, B.R., 2010. Geological interpretation of the deep seismic reflection and magnetotelluric line 08GA-OM1: Gawler craton-officer basin-Musgrave province-Amadeus basin (GOMA), south Australia and northern Territory. In: Korsch, R.J., Kositcin, N. (Eds.), GOMA (Gawler Craton-officer Basin-Musgrave Province-Amadeus Basin) Seismic and MT Workshop 2010. Geoscience Australia.
Lane, K., Jagodzinski, E.A., Dutch, R., Reid, A.J., Hand, M., 2015. Age constraints on the timing of iron ore mineralisation in the southeastern Gawler Craton. Australian Journal of Earth Sciences 62, 55–75.
Li, Z.-X., Li, X.-H., Li, W.-X., Ding, S., 2008a. Was Cathaysia part of Proterozoic Laurentia? – new data from Hainan Island, south China. Terra Nova 20, 154–164.
Li, Z.-X., Li, X.-h., Zhou, H., Kinny, P.D., 2002. Grenvillian continental collision in south China: new SHRIMP U-Pb zircon results and implications for the configuration of Rodinia. Geology 30, 163–166.
Li, Z.X., 2000. Palaeomagnetic evidence for unification of the North and West Australian cratons by ca.1.7 Ga: new results from the Kimberley Basin of northwestern Australia. Geophysical Journal International 142, 173–180.
Lo Pò, D., Braga, R., 2014. Influence of ferric iron on phase equilibria in greenschist facies assemblages: the hematite-rich metasedimentary rocks from the Monti Pisani (Northern Apennines). Journal of Metamorphic Geology 32, 371–387.
McFarlane, C.R.M., 2006. Palaeoproterozoic evolution of the Challenger Au deposit, South Australia, from monazite geochronology. Journal of Metamorphic Geology 24, 75–87.
Medig, K.P.R., Thorkelson, D.J., Davis, W.J., Rainbird, R.H., Gibson, H.D., Turner, E.C., Marshall, D.D., 2014. Pinning northeastern Australia to northwestern Laurentia in the Mesoproterozoic. Precambrian Research 249, 88–99.
Meert, J.G., 2014. Strange attractors, spiritual interlopers and lonely wanderers: the search for pre-Pangean supercontinents. Geoscience Frontiers 5, 155–166.
Merdith, A.S., Collins, A.S., Williams, S.E., Pisarevsky, S., Foden, J.D., Archibald, D.B., Blades, M.L., Alessio, B.L., Armistead, S., Plavsa, D., Clark, C., Müller, R.D., 2017. A full-plate global reconstruction of the Neoproterozoic. Gondwana Research 50, 84–134.
Middlemost, E.A., 1994. Naming materials in the magma/igneous rock system. Earth-Science Reviews 37, 215–224.
Morrissey, L.J., Hand, M., Kelsey, D.E., Wade, B.P., 2016a. Cambrian high-temperature reworking of the Rayner–Eastern Ghats terrane, constraints from the northern Prince Charles Mountains region, east Antarctica. Journal of Petrology 57, 53–92.
Morrissey, L.J., Hand, M., Lane, K., Kelsey, D.E., Dutch, R.A., 2016b. Upgrading iron-ore deposits by melt loss during granulite facies metamorphism. Ore Geology Reviews 74, 101–121.
Morrissey, L.J., Hand, M., Raimondo, T., Kelsey, D.E., 2014. Long-lived high-temperature, low-pressure granulite facies metamorphism in the Arunta Region, central Australia. Journal of Metamorphic Geology 32, 25–47.
Morrissey, L.J., Hand, M., Wade, B.P., Szpunar, M., 2013. Early Mesoproterozoic metamorphism in the Barossa complex, south Australia: links with the eastern margin of Proterozoic Australia. Australian Journal of Earth Sciences 60, 769–795.
Mulder, J.A., Halpin, J.A., Daczko, N.R., 2015. Mesoproterozoic Tasmania: Witness to the east Antarctica–Laurentia connection within Nuna. Geology 43, 759–762.
Myers, J.S., Shaw, R.D., Tyler, I.M., 1996. Tectonic evolution of Proterozoic Australia. Tectonics 15, 1431–1446.
Nance, R.D., Murphy, J.B., Santosh, M., 2014. The supercontinent cycle: a retrospective essay. Gondwana Research 25, 4–29.
Nyman, M.W., Karlstrom, K.E., 1997. Pluton emplacement processes and tectonic setting of the 1.42 Ga Signal batholith, SW USA: important role of crustal anisotropy during regional shortening. Precambrian Research 82, 237–263.
Nyman, M.W., Karlstrom, K.E., Kirby, E., Graubard, C.M., 1994. Mesoproterozoic contractional orogeny in western North America: evidence from ca. 1.4 Ga plutons. Geology 22, 901–904.
Page, R.W., Sun, S.S., 1998. Aspects of geochronology and crustal evolution in the eastern fold belt, Mt Isa Inlier. Australian Journal of Earth Sciences 45, 343–361.
Paton, C., Hellstrom, J., Paul, B., Woodhead, J., Hergt, J., 2011. Iolite: Freeware for the visualisation and processing of mass spectrometric data. Journal of Analytical Atomic Spectrometry 26, 2508–2518.
Payne, J.L., Barovich, K., Hand, M., 2006. Provenance of metasedimentary rocks in the northern Gawler craton, Australia: implications for Palaeoproterozoic reconstructions. Precambrian Research 148, 275–291.
Payne, J.L., Ferris, G., Barovich, K.M., Hand, M., 2010. Pitfalls of classifying ancient magmatic suites with tectonic discrimination diagrams: an example from the Paleoproterozoic Tunkillia Suite, southern Australia. Precambrian Research 177, 227–240.
Payne, J.L., Hand, M., Barovich, K.M., Reid, A., Evans, D.A.D., 2009. Correlations and reconstruction models for the 2500-1500 Ma evolution of the Mawson Continent. In: Reddy, S.M., Mazumder, R., Evans, D.A.D., Collins, A.S. (Eds.), Palaeoproterozoic Supercontinents and Global Evolution. Geological Society, London, Special Publications, pp. 319–355.
Payne, J.L., Hand, M., Barovich, K.M., Wade, B.P., 2008. Temporal constraints on the timing of high-grade metamorphism in the northern Gawler Craton: implications for assembly of the Australian Proterozoic. Australian Journal of Earth Sciences 55, 623–640.
Pehrsson, S.J., Eglington, B.M., Evans, D.A.D., Huston, D., Reddy, S.M., 2015. Metallogeny and its link to orogenic style during the Nuna supercontinent cycle. In: Li, Z.X., Evans, D.A.D., Murphy, J.B. (Eds.), Supercontinent Cycles through Earth History. Geological Society, London, pp. 83–94. Special Publications.
Pisarevsky, S.A., Elming, S.-Å., Pesonen, L.J., Li, Z.-X., 2014. Mesoproterozoic paleogeography: supercontinent and beyond. Precambrian Research 244, 207–225.
Powell, R., White, R.W., Green, E.C.R., Holland, T.J.B., Diener, J.F.A., 2014. On parameterizing thermodynamic descriptions of minerals for petrological calculations. Journal of Metamorphic Geology 32, 245–260.
Reddy, S.M., Evans, D.A.D., 2009. Palaeoproterozoic supercontinents and global evolution: correlations from core to atmosphere. In: Reddy, S.M., Mazumder, R., Evans, D.A.D., Collins, A.S. (Eds.), Palaeoproterozoic Supercontinents and Global Evolution. Geological Society, London, pp. 1–26. Special Publications.
Reid, A.J., Hand, M., 2012. Mesoarchean to Mesoproterozoic evolution of the southern Gawler craton, south Australia. Episodes 35, 216–225.
Reid, A.J., Jagodzinski, E.A., Armit, R.J., Dutch, R.A., Kirkland, C.L., Betts, P.G., Schaefer, B.F., 2014a. U-Pb and Hf isotopic evidence for Neoarchean and Paleoproterozoic basement in the buried northern Gawler Craton, South Australia. Precambrian Research 250, 127–142.
Reid, A.J., Jagodzinski, E.A., Fraser, G.L., Pawley, M.J., 2014b. SHRIMP U–Pb zircon age constraints on the tectonics of the Neoarchean to early Paleoproterozoic transition within the Mulgathing complex, Gawler craton, south Australia. Precambrian Research 250, 27–49.
Reid, A.J., Jagodzinski, E.A., Wade, C.E., Payne, J.L., Jourdan, F., 2017. Recognition of c. 1780Ma magmatism and metamorphism in the buried northeastern Gawler Craton: correlations with events of the Aileron Province. Precambrian Research 302, 198–220.
Ross, G.M., Parrish, R.R., Winston, D., 1992. Provenance and U-Pb geochronology of the Mesoproterozoic Belt Supergroup (northwestern United States): implications for age of deposition and pre-Panthalassa plate reconstructions. Earth and Planetary Science Letters 113, 57–76.
Ross, G.M., Villeneuve, M., 2003. Provenance of the Mesoproterozoic (1.45 Ga) Belt basin (western North America): another piece in the pre-Rodinia paleogeographic puzzle. Geological Society of America Bulletin 115, 1191–1217.
Rubenach, M.J., Foster, D.R.W., Evins, P.M., Blake, K.L., Fanning, C.M., 2008. Age constraints on the tectonothermal evolution of the Selwyn zone, eastern fold belt, mount Isa Inlier. Precambrian Research 163, 81–107.
Schmidt, P.W., Williams, G.E., Camacho, A., Lee, J.K.W., 2006. Assembly of Proterozoic Australia: implications of a revised pole for the ~1070 Ma Alcurra Dyke Swarm, central Australia. Geophysical Journal International 167, 626–634.

Selverstone, J., Hodgins, M., Aleinikoff, J.N., Fanning, C.M., 2000. Mesoproterozoic reactivation of a Paleoproterozoic transcurrent boundary in the northern Colorado Front Range: Implications for ~1.7- and 1.4-Ga tectonism. Rocky Mountain Geology 35, 139–162.

Shaw, R.D., Black, L.P., 1991. The history and tectonic implications of the Redbank Thrust Zone, central Australia, based on structural, metamorphic and Rb-Sr isotopic evidence. Australian Journal of Earth Sciences 38, 307–332.

Siddoway, C.S., Givot, R.M., Bodle, C.D., Heizler, M.T., 2000. Dynamic versus anorogenic setting for Mesoproterozoic plutonism in the Wet Mountains, Colorado: does the interpretation depend on level of exposure? Rocky Mountain Geology 35, 91–111.

Sláma, J., Košler, J., Condon, D.J., Crowley, J.L., Gerdes, A., Hanchar, J.M., Horstwood, M.S.A., Morris, G.A., Nasdala, L., Norberg, N., Schaltegger, U., Schoene, B., Tubrett, M.N., Whitehouse, M.J., 2008. Plešovice zircon — a new natural reference material for U-Pb and Hf isotopic microanalysis. Chemical Geology 249, 1–35.

Smithies, R.H., Bagas, L., 1997. High pressure amphibolite-granulite facies metamorphism in the Paleoproterozoic Rudall Complex, central Western Australia. Precambrian Research 83, 243–265.

Smithies, R.H., Howard, H.M., Evins, P.M., Kirkland, C.L., Kelsey, D.E., Hand, M., Wingate, M.T.D., Collins, A.S., Belousova, E., 2011. High-temperature granite magmatism, crust-mantle interaction and the Mesoproterozoic intracontinental evolution of the Musgrave Province, Central Australia. Journal of Petrology 52, 931–958.

Smits, R.G., Collins, W.J., Hand, M., Dutch, R., Payne, J.L., 2014. A Proterozoic Wilson cycle identified by Hf isotopes in central Australia: implications for the assembly of Proterozoic Australia and Rodinia. Geology 42, 231–234.

Spaggiari, C.V., Kirkland, C.L., Smithies, R.H., Wingate, M.T.D., Belousova, E.A., 2015. Transformation of an Archean craton margin during Proterozoic basin formation and magmatism: the Albany–Fraser orogen, western Australia. Precambrian Research 266, 440–466.

Spikings, R.A., Foster, D.A., Kohn, B.P., Lister, G.S., 2002. Post-orogenic (<1500 Ma) thermal history of the Palaeo-Mesoproterozoic, Mt. Isa province, NE Australia. Tectonophysics 349, 327–365.

Stevens, B.P.J., Page, R.W., Crooks, A., 2008. Geochronology of Willyama supergroup metavolcanics, metasediments and contemporaneous intrusions, Broken Hill, Australia. Australian Journal of Earth Sciences 55, 301–330.

Stewart, E.D., Link, P.K., Fanning, C.M., Frost, C.D., McCurry, M., 2010. Paleogeographic implications of non–north American sediment in the Mesoproterozoic upper belt supergroup and Lemhi Group, Idaho and Montana, USA. Geology 38, 927–930.

Swain, G., Barovich, K., Hand, M., Ferris, G., Schwarz, M., 2008. Petrogenesis of the St peter suite, southern Australia: Arc magmatism and Proterozoic crustal growth of the south Australian craton. Precambrian Research 166, 283–296.

Swain, G., Woodhouse, A., Hand, M., Barovich, K., Schwarz, M., Fanning, C.M., 2005a. Provenance and tectonic development of the late Archaean Gawler Craton, Australia; U–Pb zircon, geochemical and Sm–Nd isotopic implications. Precambrian Research 141, 106–136.

Swain, G.M., Hand, M., Teasdale, J., Rutherford, L., Clark, C., 2005b. Age constraints on terrane-scale shear zones in the Gawler Craton, southern Australia. Precambrian Research 139, 164–180.

Szpunar, M., Hand, M., Barovich, K., Jagodzinski, E., Belousova, E., 2011. Isotopic and geochemical constraints on the Paleoproterozoic Hutchison Group, southern Australia: implications for Paleoproterozoic continental reconstructions. Precambrian Research 187, 99–126.

Thomas, J.L., Direen, N.G., Hand, M., 2008. Blind orogen: Integrated appraisal of multiple episodes of Mesoproterozoic deformation and reworking in the Fowler Domain, western Gawler Craton, Australia. Precambrian Research 166, 263–282.

Tucker, N.M., Hand, M., Kelsey, D.E., Dutch, R.A., 2015. A duality of timescales: short-lived ultrahigh temperature metamorphism preserving a long-lived monazite growth history in the Grenvillian Musgrave–Albany–Fraser Orogen. Precambrian Research 264, 204–234.

Tucker, N.M., Morrissey, L.J., Payne, J.L., Szpunar, M., 2018. Genesis of the Archean–Paleoproterozoic Tabletop domain, Rudall province, and its endemic relationship to the west Australian Craton. Australian Journal of Earth Sciences. https://doi.org/10.1080/08120099.2018.1479307 (in press).

Li, Z.X., Bogdanova, S.V., Collins, A.S., Davidson, A., De Waele, B., Ernst, R.E., Fitzsimons, I.C.W., Fuck, R.A., Gladkochub, D.P., Jacobs, J., Karlstrom, K.E., Lu, S., Natapov, L.M., Pease, V., Pisarevsky, S.A., Thrane, K., Vernikovsky, V., 2008b. Assembly, configuration, and break-up history of Rodinia: a synthesis. Precambrian Research 160, 179–210.

Vassallo, J.J., Wilson, C.J.L., 2002. Palaeoproterozoic regional-scale non-coaxial deformation: an example from eastern Eyre Peninsula, South Australia. Journal of Structural Geology 24, 1–24.

Verbaas, J., Thorkelson, D.J., Crowley, J., Davis, W.J., Foster, D.A., Gibson, H.D., Marshall, D.D., Milidragovic, D., 2018. A sedimentary overlap assemblage links Australia to northwestern Laurentia at 1.6 Ga. Precambrian Research 305, 19–39.

Wade, B.P., Hand, M., Barovich, K.M., 2005. Nd isotopic and geochemical constraints on provenance of sedimentary rocks in the eastern Officer Basin, Australia: implications for the duration of the intracratonic Petermann Orogeny. Journal of the Geological Society 162, 513–530.

Wade, B.P., Payne, J.L., Hand, M., Barovich, K.M., 2007. Petrogenesis of ca 1.50 Ga granitic gneiss of the Coompana Block: filling the 'magmatic gap' of Mesoproterozoic Australia. Australian Journal of Earth Sciences 54, 1089–1102.

Wade, C.E., Reid, A.J., Wingate, M.T.D., Jagodzinski, E.A., Barovich, K., 2012. Geochemistry and geochronology of the c. 1585Ma Benagerie Volcanic Suite, southern Australia: relationship to the Gawler Range Volcanics and implications for the petrogenesis of a Mesoproterozoic silicic large igneous province. Precambrian Research 206–207, 17–35.

Walsh, A.K., Kelsey, D.E., Kirkland, C.L., Hand, M., Smithies, R.H., Clark, C., Howard, H.M., 2015. P–T–t evolution of a large, long-lived, ultrahigh-temperature Grenvillian belt in central Australia. Gondwana Research 28, 531–564.

Webb, A.W., Thomson, B.P., Blissett, A.H., Daly, S.J., Flint, R.B., Parker, A.J., 1986. Geochronology of the Gawler craton, south Australia. Australian Journal of Earth Sciences 33, 119–143.

Whalen, J.B., Currie, K.L., Chappell, B.W., 1987. A-type granites: geochemical characteristics, discrimination and petrogenesis. Contributions to Mineralogy and Petrology 95, 407–419.

White, R.W., Powell, C.M., Halpin, J.A., 2004. Spatially-focussed melt formation in aluminous metapelites from Broken Hill, Australia. Journal of Metamorphic Geology 22, 825–845.

White, R.W., Powell, R., Clarke, G.L., 2002. The interpretation of reaction textures in Fe-rich metapelitic granulites of the Musgrave Block, central Australia: constraints from mineral equilibria calculations in the system K2O–FeO–MgO–Al2O3–SiO2–H2O–TiO2–Fe2O3. Journal of Metamorphic Geology 20, 41–55.

White, R.W., Powell, R., Holland, T.J.B., Johnson, T.E., Green, E.C.R., 2014a. New mineral activity–composition relations for thermodynamic calculations in metapelitic systems. Journal of Metamorphic Geology 32, 261–286.

White, R.W., Powell, R., Holland, T.J.B., Worley, B.A., 2000. The effect of TiO2 and Fe2O3 on metapelitic assemblages at greenschist and amphibolite facies conditions: mineral equilibria calculations in the system K2O-FeO-MgO-Al2O3-SiO-H2O-TiO-Fe2O3. Journal of Metamorphic Geology 18, 497–511.

White, R.W., Powell, R., Johnson, T.E., 2014b. The effect of Mn on mineral stability in metapelites revisited: new a–x relations for manganese-bearing minerals. Journal of Metamorphic Geology 32, 809–828.

Whitmeyer, S.J., Karlstrom, K.E., 2007. Tectonic model for the Proterozoic growth of north America. Geosphere 3, 220–259.

Wiedenbeck, M., AllÉ, P., Corfu, F., Griffin, W.L., Meier, M., Oberli, F., Quadt, A.V., Roddick, J.C., Spiegel, W., 1995. Three natural zircon standards for U-Th-Pb, Lu-Hf, trace element and REE analyses. Geostandards Newsletter 19, 1–23.

Wingate, M.T.D., Evans, D.A.D., 2003. Palaeomagnetic constraints on the Proterozoic tectonic evolution of Australia. In: Yoshida, M., Windley, B.F., Dasgupta, S. (Eds.), Proterozoic East Gondwana: Supercontinent Assembly and Breakup. Geological Society, London, Special Publications, pp. 77–91.

Yang, B., Smith, T.M., Collins, A.S., Munson, T.J., Schoemaker, B., Nicholls, D., Cox, G., Farkas, J., Glorie, S., 2018. Spatial and temporal variation in detrital zircon age provenance of the hydrocarbon-bearing upper roper group, beetaloo sub-basin, Northern Territory, Australia. Precambrian Research 304, 140–155.

Zhang, S., Li, Z.-X., Evans, D.A.D., Wu, H., Li, H., Dong, J., 2012. Pre-Rodinia supercontinent Nuna shaping up: a global synthesis with new paleomagnetic results from North China. Earth and Planetary Science Letters 353–354, 145–155.

Zhao, G., Cawood, P.A., Wilde, S.A., Sun, M., 2002. Review of global 2.1–1.8 Ga orogens: implications for a pre-Rodinia supercontinent. Earth-Science Reviews 59, 125–162.

Zhao, G., Sun, M., Wilde, S.A., Li, S., 2004. A Paleo-Mesoproterozoic supercontinent: assembly, growth and breakup. Earth-Science Reviews 67, 91–123.